POLSKA AKADEMIA NAUK
INSTYTUT FIZYKI
POLSKIE TOWARZYSTWO FIZYCZNE

ACTA PHYSICA POLONICA

MIESIĘCZNIK

Vol. XX — Fasc. 2

WARSZAWA 1961

PAŃSTWOWE WYDAWNICTWO NAUKOWE

PAŃSTWOWE WYDAWNICTWO NAUKOWE — Oddział w Krakowie
Kraków, ul. Smoleńsk 14

Nakład 918 + 152 egz.	*Podpisano do druku 14 marca 1961*
Ark. wyd. 5,5, ark. druk. 5¼	*Druk ukończono w marcu 1961*
Papier druk. sat. 80 g kl. III, 70×100 cm	*Zamówienie prod. 603/60*
Oddano do składania 2 listopada 1960	*Cena zł 30,—*

DRUKARNIA NARODOWA W KRAKOWIE, ul. Manifestu Lipcowego 19

STRUCTURE OF ETCHING FIGURES ON BISMUTH SELENIDE SINGLE CRYSTALS

By B. Kołakowski

Institute of Physics, Polish Academy of Sciences, Warsaw

(*Received June 6, 1960; translated paper received on August 6, 1960*)

The formation of etching figures on the (0001) face of bismuth selenide single crystals is investigated. Different etching mixtures were found to give rise to figures of different shape and density of distribution. The mixture best adapted for the detection of dislocations was that (No. 5) containing bromine and iodine. In order to explain the different forms and densities of the figures, depending on the procedure of etching, a model is proposed wherein the walls of the etching figures are considered to consist of an assemblage of steps. The model relates the thickness of the steps to the form and orientation of the figures and to the rate of etching.

Recently, a number of papers on methods of revealing details of the defect structure of crystals have been published.

One of the most involved and least elucidated problems is that of dissolving the crystal. This process often leads to widely different results according to the defects present in the crystal, the type of structure and the method used. Maybe the etching figures formed at the intersections of dislocations with the crystal surface are the most readily interpreted.

The present investigation aimed at interpreting problems of this type in the case of semiconducting bismuth selenide crystals of purity corresponding to 8×10^{18} — -2×10^{19} holes per cm^3 (type p), etched chemically.

In order to obtain insight into the process of formation of various figures according to the conditions of dissolving, a number of etching substances were utilized. Thus, the effect of small admixtures to the etching solution on the form of the figures obtained on the crystal surfaces was detected.

The experimental procedure is the following: Plates of bismuth selenide obtained by splitting along the (0001) plane were immersed in the etching solution for two minutes, rinsed in ethanol and dried. The plates were etched at room temperature; if etching was continued, the temperature of the crystals rose and the figures obtained in the process of etching were not easily reproducible. The preparates thus obtained

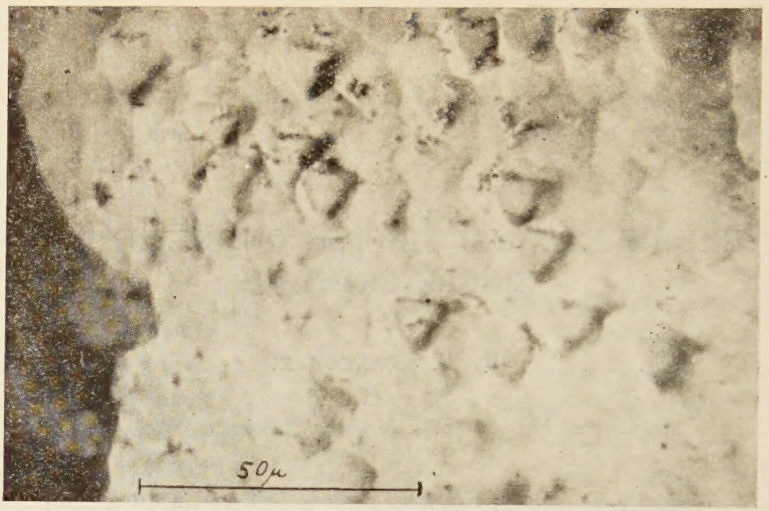

Picture 1

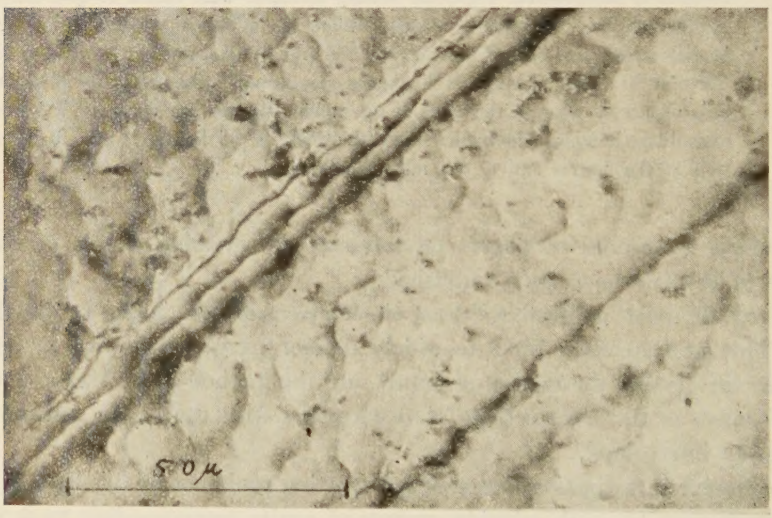

Picture 2

were subjected to observation with a metallographic microscope and micro-interferometer magnifying 120 to 1400 times.

The form of the etching figures varied according to the solution used. The composition of the latter is given at the end of the present paper, for the various cases.

If mixture No. 1 was used, the figures obtained did not exhibit the symmetry characteristic of the crystal face considered.

With mixture No. 2, a more distinct picture of the figures was obtained; this consisted of triangular pits whose edge was about 7μ long, and which were distributed

Picture 3

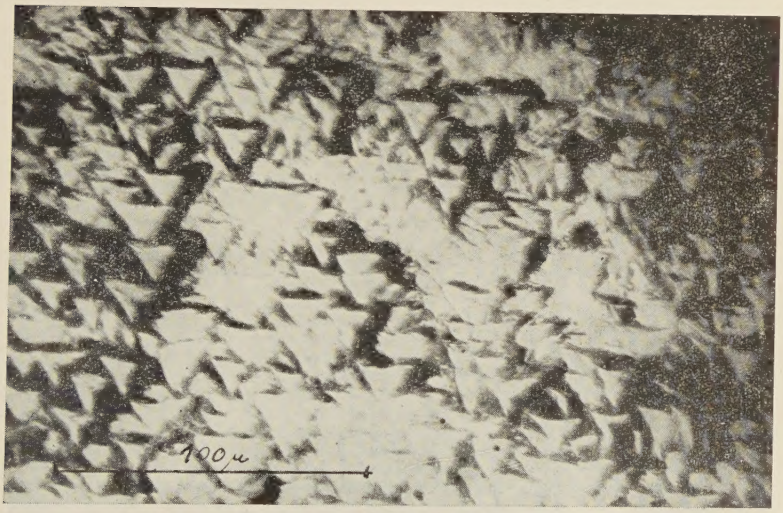

Picture 4

with a density of the order of 10^8 per cm^2. The pits were flat and, in some regions, were arrayed in rows. The formation of the pits proceeded as long as etching went on, at first presenting a triangular shape and then rounding, finally to become diffluent. The density of the pits having sharply defined edges was constant throughout etching. This would seem to indicate that these figures derive from defects of rather small linear dimensions and lattice irregularities distributed evenly throughout the crystal.

Picture 1 presents single etching figures of different shapes possessing or not the triangular symmetry.

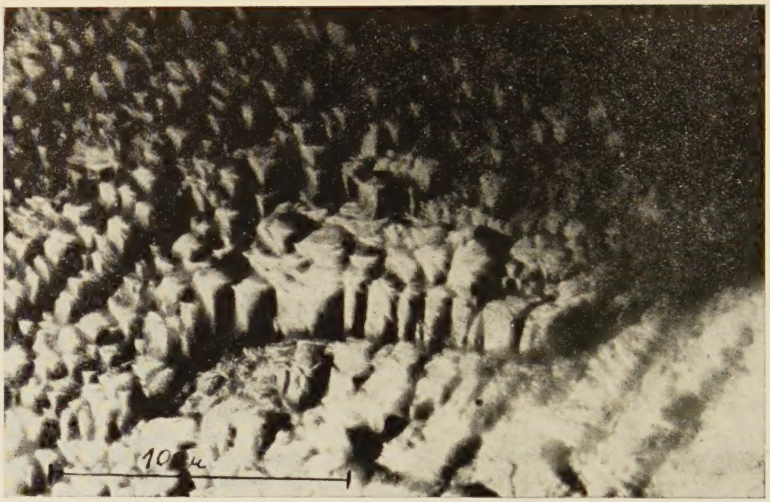

Picture 5

Picture 6

Picture 2 shows etched slip bands, this fact was established as the result of complementary X-ray studies.

Some regions exhibit rows of etch pits forming a lattice of triangular lattice points (Picture 3). Most probably, these are boundaries between blocks rotated mutually by a small angle.

Etching mixture No. 3 yielded faces covered with triangular figures outlined sharply. Picture 4 shows the (0001) crystal face on etching with this mixture. Some

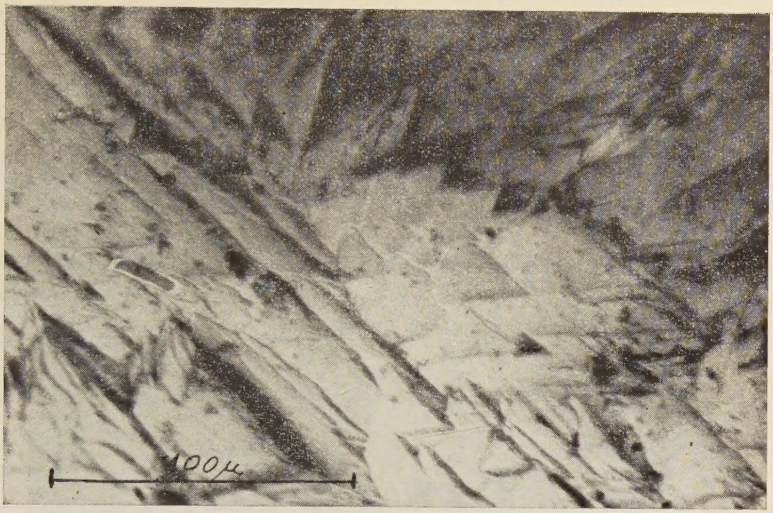

Picture 7a

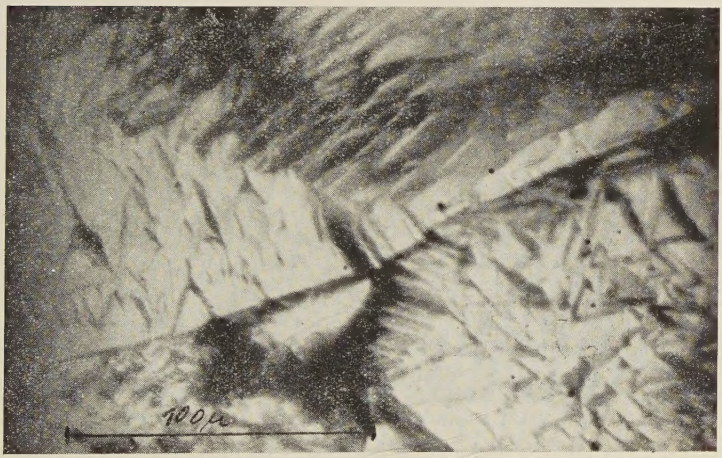

Picture 7b

figures are seen to be arranged in larger ones of the same shape and symmetry. Picture 5 shows etch pits grouped in rows.

Mixture No. 4 yielded etching figures resembling though somewhat more contrasty than those obtained with No. 3: the single figures were very sharply outlined, whereas the groups of small figures covered larger areas and partook of the character of large cavities of complex structure reminiscent of the figures observed by Oberly on germanium (Oberly 1957).

Picture 6 is that of the surface of a Bi_2Se_3 crystal subjected to etching with mixture No 4, showing either kind of figures.

Pictures 7a and 7b show the structure of the large cavities of Picture 6 at greater enlargement.

Mixture No 5. also yielded two kinds of figures having sharp contours and the symmetry corresponding to the crystal face subjected to etching: the large ones appearing sporadically, and the small ones distributed densely. The large pits resulted from deformation in the crystals investigated; they sometimes appeared in rows (Picture 14).

X-ray investigation according to Dr J. Auleytner's method (Auleytner 1958) and utilizing a point source of X-rays with focus diameter of about 20μ (Auleytner 1957) established that the large pits appear at the boundaries of mutually

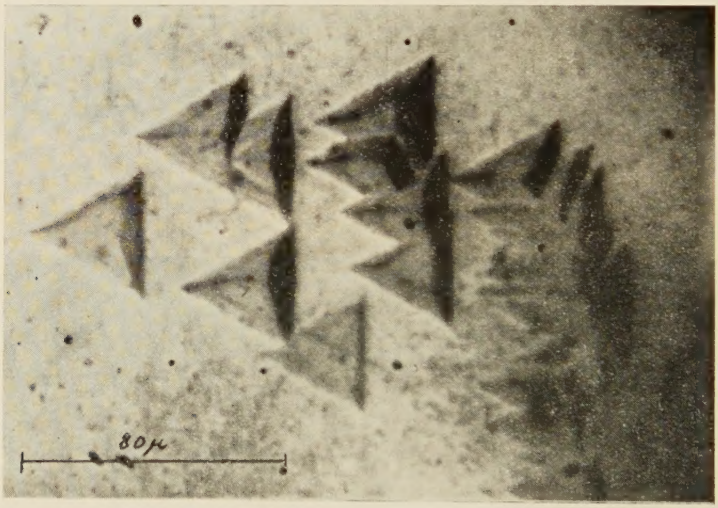

Picture 8

rotated regions, corresponding to sites at which the dislocations intersect with the crystal surface.

Picture 8 shows a crystal surface covered with a group of dislocation etch pits, whereas Picture 9 is that of a dislocation boundary terminating in a group of disordered dislocations.

In order to investigate more closely the surface etched in mixture No. 5, a number of photographs were taken utilizing a microinterferometer. This led to a more exact determination of shape and structure as well as of the depth and angle of inclination of the walls bounding the pits. The walls of the pits formed an angle ranging from 6° to 9° with the crystal surface, the maximum depth attaining about 6μ, whereas that of the small pits amounted to about 0.4 μ.

Moreover, the pictures obtained with the microinterferometer served to establish the depth of the inequalities on the surfaces subjected to etching, in the regions presenting no pits of either kind. Fluctuations of the inequalities of the surface between cavities amounted to some tenth of a micron.

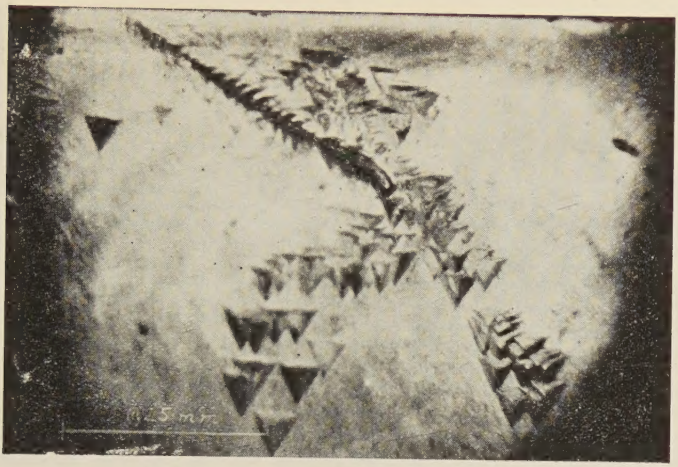

Picture 9

Picture 10

Picture 10 is that of a region covered with small etch pits.

Picture 11 shows separate large etch pits arising from dislocations presenting different angles of inclination with respect to the crystal surface of the walls bounding them. Hence it is to be inferred that the dislocation lines giving rise to the pits were inclined with respect to the crystal surface at an angle other than 90°.

When observing the distribution of the interference fringes on the surface of the walls bounding the etch pits, it is seen that the angle at which they are inclined with respect to the crystal surface varies. Hence it is to be concluded that the dislocations giving rise to the cavities in the process of etching were of varying inclination throughout a layer whose thickness equals that of the cavity.

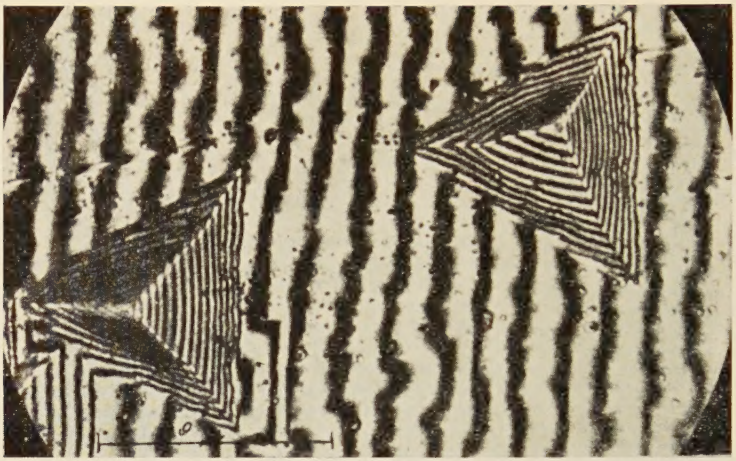

Picture 11

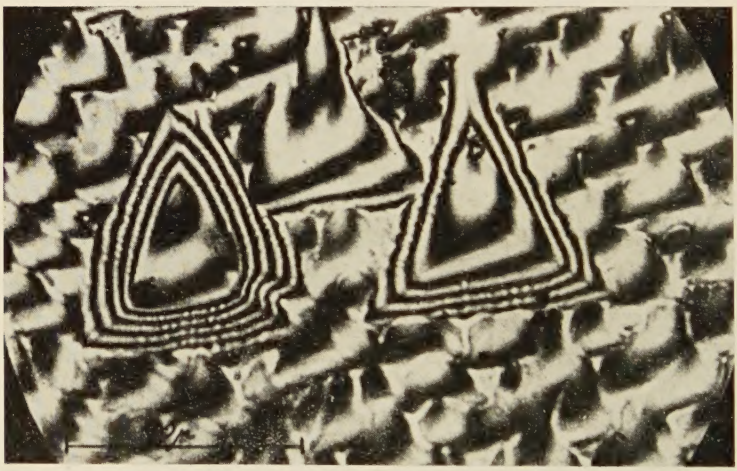

Picture 12

Picture 12 shows large etch pits of flat bottom, deriving from dislocations. This may result from abrupt curvature of the dislocation lines (Yamamoto 1958).

Picture 13 shows some groupings of pits corresponding to dislocation lines.

Picture 14 represents an etched dislocation boundary. The regular distribution of the dislocation pits along the boundary is clearly visible. The interference fringes point to an angle of inclination of the latter with respect to the crystal surface differing from 90°.

In all cases, the surfaces bounding the pits were found to belong to the same type of crystallographic form.

In considering the process of etching, the rate of etching is sometimes represented as the sum of a component normal and of one tangent to the surface subjected to

Picture 13

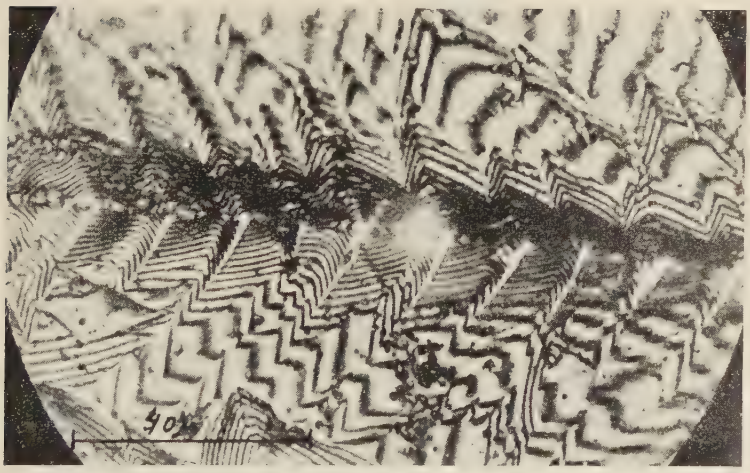

Picture 14

etching (cf., e.g., Yamamoto 1958, Gilman et al. 1958). This procedure is especially well adapted to the case of the (0001) face of bismuth selenide crystals, as the latter present a layer structure involving considerable anisotropy of their properties. This is especially salient when the *c*-axis direction is compared with the directions perpendicular thereto.

The rate of etching depends on the energy of the bonds retaining the atoms on the crystal surface. If a step is formed on the (0001) face, the rate of etching in the tangential directions will greatly exceed that in the normal direction, since the atoms on the edge of the step are much more loosely attached to the crystal than those on the (0001) face,

Hence, the etching rate may be said quite generally to depend on two factors, namely:

1) the rate of formation of monatomic pits, and

2) the etching rate in the tangential directions.

Either factor depends on the energy per single bond of the atoms forming the crystal surface. The reaction rate of etching is, among others, a function of $\exp(E/kT)$, wherein E denotes the activation energy dependent on the energy of the bonds of a given lattice point on the crystal surface.

Taking into account the ratios of the etching rates for the various possible crystal faces, it is obvious that, as the temperature rises, the rates of etching of the different faces and edges will tend to assume one value. Thus, a rise in the activation energy will, on the one hand, diminish the etching rate and, on the other, enhances the anisotropy of etching.

Detailed consideration of the structure of the Bi_2Se_3 crystals investigated yields an explanation of the different forms and densitites of the etching figures depending on the method of etching employed. Bismuth selenide crystallizes in the trigonal system, in the space group $D^5_{3d} = R\bar{3}m$ (Semilyetov 1954). The basis of the Bi_2Se_3 crystal structure is given by nine layers of selenium atoms disposed according to the symmetry of the trigonal system

$$...ABACBCACA...$$

wherein the bismuth atoms occupy two thirds of the octahedric interstices

$$AcBAcBAcBaCbACbA...$$

Taking into account the layers transforming into themselves by translation, we have

$$...\bar{A}\bar{B}\bar{C}\bar{A}\ ...$$

On the (0001) face of crystals possessing such structure, etching can lead to the formation of two kinds of differently oriented pits. The pits of either kind have edges wherein the density of atom setting is the greatest.

In order to distinguish pits of different kinds and the same configuration, one kind will be denoted by L, and the other by the letter P.

Fig. 1 represents a single layer, showing the direction of the bonds with the next and the preceding layer wherein two pits are present: one of configuration L, and the other one of configuration P. In the circles denoting atoms or molecules, blank fields represent bondings with the upper layer, black ones — with the lower layer, and bondings with neighbouring atoms within the layer are symbolized by the boundaries between the black and blank fields. From Fig. 1, pits of either configuration are seen to be equally possible if they are of monomolecular depth, as then the atoms on their edges are equally strongly bonded to the base. If, however, the etch pits become deeper conditions can arise when their walls will consist of steps many layers thick.

According to the structure of the pits' walls, the etching rates for cavities of either configuration can undergo differentiation or can remain equal. This depends on the distances and thickness of the steps bounding them.

The following cases can occur:

1) the pits can be bounded by mutually separate steps of monomolecular thickness,
2) the pits can be bounded by mutually separate steps of thickness exceeding that of one layer (Fig. 2), or
3) the pits can be bounded by surfaces exhibiting no steps.

In the case of (1), as in that of the monomolecular pit, both configurations are equally possible. As a results of this, the etching figures can assume a macroscopically

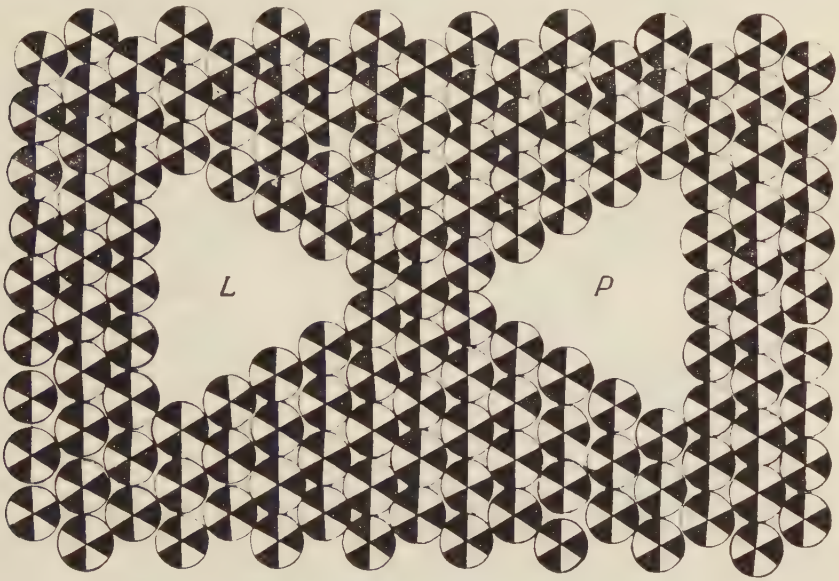

Fig. 1. Two equally probable antisymmetric etching figures on the (0001) face, of depth equalling the thickness of a single layer.
The circles represent atoms: blank fields denote bonds directed upwards, black fields denote bondings with the neighbouring lower layer (omitted for clarity), and the black/blank boundaries denote bondings with neighbouring atoms in the same layer.
The atoms on the edges in either figure (*L* and *P*) are seen to be equally strongly attached to the crystal.

more or less regular shape not related to the crystallographic symmetry of the surface wherein they are present. This case can serve for describing the figures obtained in etching with mixture No. 1.

In the case of (2), the pits obtained by etching would present walls constructed of mutually separate steps of thickness greater than that of a single layer. Fig. 2 shows two pits of configuration *L* and *P*, of the depth of one two-layer steps.

The bonds attaching the atoms of the edges of the upper layer forming the upper surface of the step to the substratum are seen to be equally strong in the case of either pit; however, the atoms on the edge of the next layer in either pit are bonded to the substratum with different strength (it should be held in mind that, on the circles denoting atoms or molecules, blank fields represent bondings with the upper layer, black ones — with the lower layer, and bondings with neighbours in the same layer are symbolized by the boundaries between black and blank fields).

From Fig. 2, the atoms on the edges of the layer immediately beneath the upper one are less strongly attached to the substratum in the case of configuration *L* than in that of configuration *P*. In case *L*, the edge of the layer underlying the upper one contains atoms having two non-saturated bondings with neighbouring atoms and two with atoms of the upper layer, whereas in case *P* the same atoms present two non-saturated bondings with neighbouring atoms and one with those of the upper layer. Hence, the etching rate for the lateral walls of the steps in configuration *L* should

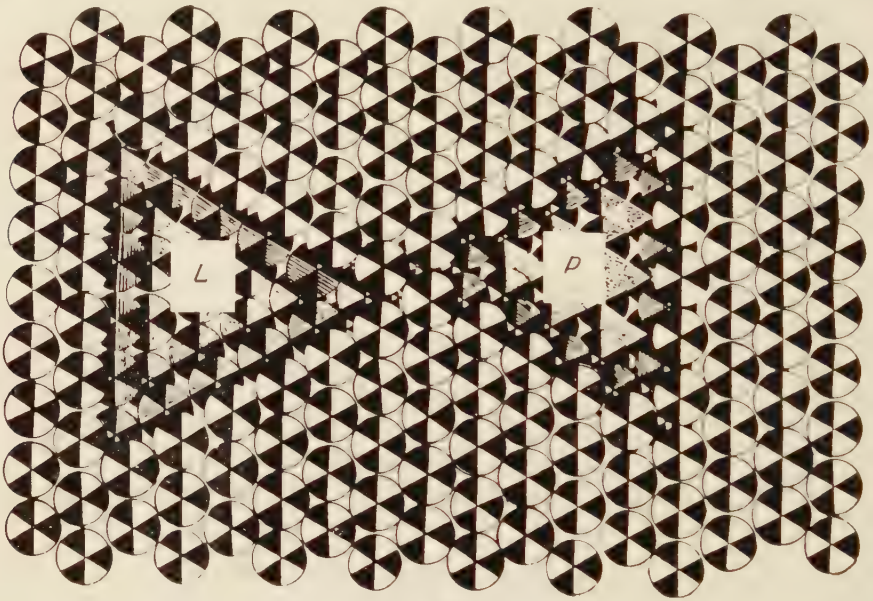

a

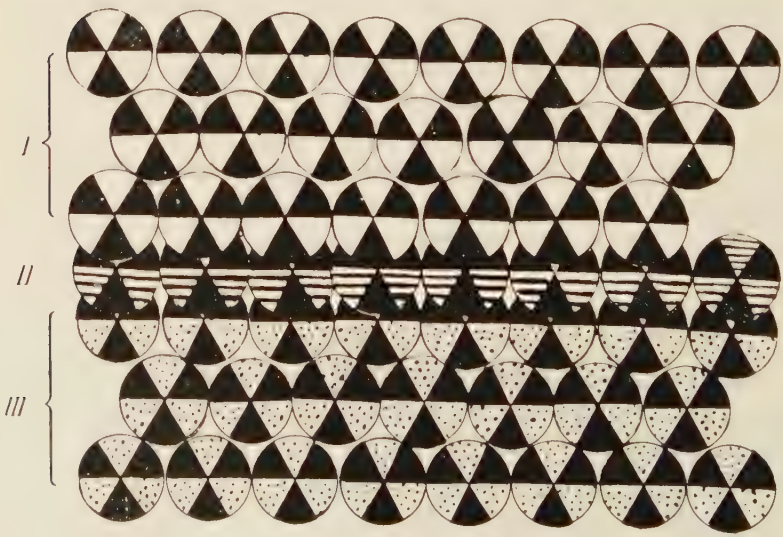

b

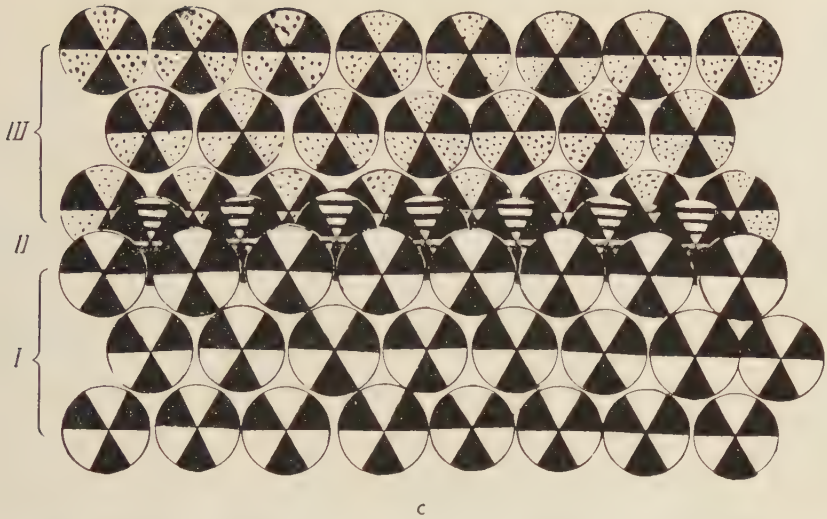

Fig. 2. a) Pits of the same configurations as in Fig. 1, albeit of increased depth and exhibiting the formation of a step of the thickness of two layers.

The notations is that of Fig. 1, the atoms of the upper layer (forming the crystal face etched) being represented by blank fields (I), the atoms of the following layer (II) — by blank shaded fields, and the blank fields of the atoms in the layer constituting the bottom of the pit (III) are dotted.

It is seen that, although the atoms on the edge of the upper layer are equally strongly bonded to the substratum in either configuration of the pit, those on the edge of the underlying layer are less strongly attached in configuration *L* than in configuration *P*. This explains why the crystal, on etching, exhibits pits of configuration *P* only.

b) Section of *L* cavity.

c) Section of *P* cavity.

exceed that for configuration *P*, and the etch pits should be expected to assume configuration *P*. Moreover, it is obvious that, as the thickness of the steps increases, so will also the differences between the etching rates for the lateral walls of the steps in either configuration of the pits. Simultaneously, the etching rate of the lateral walls of the steps in either configuration will diminish, since then the density of step edges per unit depth of the figure etched diminishes, and the atoms on the edges are those that are the least strongly attached to the substratum.

Case (3) can be said to represent the limit for case (2) with the pit walls constituting a homogeneous step surface and the three walls being crystallographic planes inclined at a constant angle with respect to the crystal surface subjected to etching.

From the model proposed it may be concluded that, as the etch pits assume forms that are progressively sharper, the etching rate of the crystal should decrease, and, moreover, that all cavities should have the same orientation, as was indeed the fact when applying mixtures Nos. 1—5.

At the same time, further observation established that the pits should possess a structure consisting of steps of a thickness of several layers, and not be bounded by surfaces devoid of steps. This results from the interferograms, which point to pits

bounded by surfaces of variable inclination with respect to the crystal surface, proving that case (3) cannot occur. Obviously, the model proposed, wherein the wall is considered to consist of an array of steps, can also be adapted to crystals belonging to systems other than bismuth selenide.

From the variable inclination of the surfaces bounding the etch pits, the dislocations pervading the crystal can be concluded to have been curvilinear (Yamamoto 1958). However, the angle of inclination of the dislocations accounting for the formation of the pits cannot be determined unless the angular distribution of the etching rate is known.

Investigation of the effect of admixtures of bromine and iodine to the etching liquid suggests that bromine and iodine raise the activation energy, thus leading to a differentiation of the size of the etch pits, and that they may enhance the formation of multi-layer steps.

Results

1) The effect of various etching mixtures on the microscopic structure of the etched surfaces of bismuth selenide single crystals was investigated.
2) Etching mixtures Nos. 1—5 were found to produce different etching figures, the density and shape thereof varying according to the mixture used.
3) The addition of bromine and iodine to the etching mixtures was found to produce etching figures possessing sharper outlines; moreover, the figures, then fall in two classes, namely, densely disposed minute pits, and large ones of a dislocational origin. Hence, bromine and iodine can be said to be factors influencing the contrastiness of the picture.
4) Mixture No. 5 was found to yield the best results in revealing dislocations.
5) An explanation is proposed for the fact that a single type of pits is observed on the crystals etched, on the basis of the structural data for bismuth selenide.
6) The mechanism of etching is discussed on the basis of the experimental results obtained and with respect to the model proposed, which is applicable to crystals of other systems also.

Etching mixtures applied:

No. 1: 2 parts of HNO_3
1 part of HCl
1 part of H_2O_2

No. 2: 2 parts of HNO_3
1 part of HCl
1 part of H_2O_2

No. 3: 2 parts of HNO_3
1 part of HCl
Br_2 to saturation

No. 4: 2 parts of HNO_3
1 part of HCl
1 part of C_2H_5OH
J_2 to saturation

No. 5: 2 parts of HNO_3
1 part of HCl
1 part of C_2H_5OH
Br_2 and J_2 to saturation

The author wishes to thank Professor Dr L. Sosnowski for his detailed discussions and valuable comments, Dr J. Auleytner for his decisive remarks and advice, Mr. W. Chlebowski, B. Sc., for providing the bismuth selenide crystals, and Mr J. Raułuszkiewicz, B. Sc., for determining their degree of purity.

REFERENCES

Auleytner, J., *Acta phys. Polon.*, **17**, 111 (1958).
Auleytner, J., *Acta phys. Polon.*, **16**, 35 (1957).
Gilman, J., Johnston, W. and Sears, G., *J. appl. Phys.*, **29**, 747 (1958).
Semilyetov, *Kristallografia*, 1954.
Yamamoto, M., *Sci. Rep. Res. Insts. Tohoku Univ., Series A* — Feb. 1 (1958).

EINFLUSS VON FLÜSSIGKEITEN AUF DIE TRIBOERREGUNG DES ALUMINIUMS ZUR PHOTOSTIMULIERTEN EXOELEKTRONENEMISSION

Von T. Lewowski und B. Sujak*

Institut für Experimentalphysik der Universität, Wrocław

(Eingegangen am 7 Juni, 1960)

Der Einfluss von Flüssigkeiten auf die Triboerregung des Aluminiums zur Exoelektronenemission wurde untersucht. Die Intensität dieser Emission wurde bei Beleuchtung mit weissen Licht einer Wolframlampe mit Hilfe eines offenen Luftspintzenzählers gemessen. Die untersuchten (vorwiegend organischen) Flüssigkeiten zeigten einen unterschiedlichen Einfluss auf die Triboerregung je nach der Erregungsart: Bürsten mit einer Stahlbürste oder Abschabung mit einer Feile (auch Messerkante). Im Falle der Bearbeitung der Oberfläche mit einer Stahlbürste lassen sich die untersuchten Flüssigkeiten in drei Gruppen einteilen: 1) diejenigen die stärker löschend auf die Triboerregung wirken als die Luftatmosphäre, 2) diejenigen die milder löschend wirken und 3) diejenigen die den gleichen Einfluss auf die Triboerregung wie die Luftatmosphäre zu zeigen scheinen. Die Moleküle der Flüssigkeiten der ersten Gruppe enthalten sowohl Sauerstoff- als auch Wasserstoffatome, die der zweiten Gruppe nur Wasserstoffatome. In den Molekülen der Flüssigkeiten der dritten Gruppe sind weder Wasserstoff- noch Sauerstoffatome vorhanden. Im Falle der Abschabung der Oberfläche mit einer Feile oder einer Messerkante wirkten dagegen alle untersuchten Flüssigkeiten stets mehr oder weniger stärker löschend als die Luftatmosphäre.

Um den Einfluss der Flüssigkeiten auf die Triboerregung gut verfolgen zu können, musste der Kontakt Aluminium-Flüssigkeit in einer möglichst kurzen Zeit nach der Oberflächenbearbeitung stattfinden. Der Einfluss von elektrischen Strömen in den Flüssigkeiten auf die Triboerregung der Aluminiumelektroden wurde orientierungsweise auch untersucht. Es zeigte sich, dass je nach der gewählten Stromrichtung eine elektrolytische Erregung oder Auslöschung der photostimulierten Exoelektronenemission stattfinden kann.

Die chemische Wirkung der an der Kontaktoberfläche sich zersetzenden Moleküle wird als Ursache des Einflusses der Flüssigkeiten auf die Triboerregung zur photostimulierten Exoelektronenemission gedeutet.

Einführung

In unserer Arbeitsgruppe wurden verschiedene Oxydationsprozesse an Aluminiumoberflächen mit Hilfe der Exoelektronenemission untersucht. Es wurde dabei unter anderen festgestellt, dass durch das Spülen der Proben mit Wasser die Tri-

* Zur Zeit in The Clarendon Laboratory, Oxford

boerregung zur Exoelektronenemission in kürzester Zeit beträchtlich erniedrigt werden kann. Diese löschende Wirkung des Wassers, die Benutzung von Ätzverfahren bei den Untersuchungen von Exoelektronenemission, sowie das Problem der Elektronenemission in Flüssigkeiten im allgemeinen, haben uns veranlasst die Einwirkung von Flüssigkeiten auf die mechanische Erregung zur Exoelektronenemission näher zu verfolgen. Die vorliegende Arbeit enthält einen Bericht über die Ergebnisse dieser Untersuchung an Oberflächen des technischen Aluminiums in einer schematischen Darstellung. Die Ergebnisse scheinen auch für Korosionsfragen der deformierten Metalle von Bedeutung zu sein (Thomson 1958).

Untersuchungsmethode

Zur Untersuchung der Einwirkung von Flüssigkeiten auf die Triboerregung zur photostimulierten Exoelektronenemission (die weiterhin als Ph. Ex. Em. bezeichnet wird) wurden Proben aus technischem Aluminium vorbereitet. Die Länge der Proben betrug etwa 8 cm, die Breite etwa 2 cm die Dicke 0,2 cm.

Ein Teil der Proben wurde mit einer Stahlbürste oberflächlich bearbeitet. Der andere Teil dagegen wurde mit Hilfe einer groben Stahlfeile oder eines Stahlmessers abgeschabt. Die Bearbeitung der Oberfläche erfolgte immer in atmosphärischer Luft unter Tageslicht. Kurz nach erfolgter Bearbeitung der Oberfläche wurde die Verteilung der Emissionsitensität der Ph. Ex. Em. entlang der ganzen Probe gemessen. Dieses Abtasten der Proben geschah in Dunkelheit mit Hilfe eines offenen Luftspitzenzählers durch welchen hindurch das weisse Licht einer Wolframlampe die untersuchte Stelle der Proben beleuchtete (Sujak 1957, Mader und Sujak, 1960). Somit wurden für jede Probe die Abtastkurven $N/t = f(x)$ der Ph. Ex. Em. aufgenommen. Die benutzte Messanordnung ist in Abb. 1. schematisch wiedergegeben.

Zur weiteren Untersuchung gelangten nur Proben deren Abtastkurven einen gleichmässigen und horizontalen Verlauf zeigten. Diese wurden danach in der gewählten Flüssigkeit (Raumtemperatur) teilweise für etwa 5 Sekunden eingetaucht, in

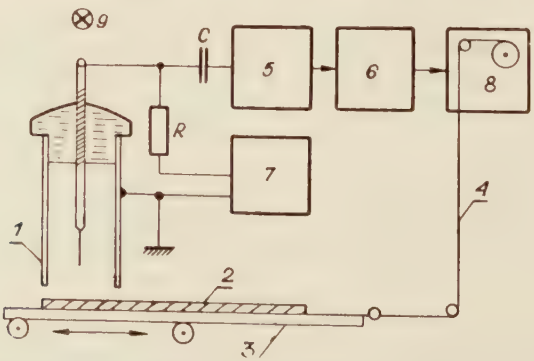

Abb. 1. Schematische Darstellung der Messanordnung: (1) Spitzenzähler, (2) Al-Probe, (3) Bewegliche Probenunterlage, (4) Papierband-Kuppelung, (5) Verstärker, (6) Impulsmittelmesser, (7) Hochspannungsspeisegerät, (8) Selbstschreibegerät zur Aufzeichnung der Ph. Ex. Em. Abtastkurven, (9) Lichtquelle

kaltem Luftstrom (Raumtemperatur) getrocknet und die Abtastkurven der Ph. Ex. Em. wurden dann wieder aufgenommen. In sämtliche Abbildungen wurden die Abtastkurven der Ph. Ex. Em., die nach der mechanischen Bearbeitung aufgenommen wurden, gestrichelt eingezeichnet. Voll ausgezogen wurden dagegen die Abtastkurven, die nach der Einwirkung der angegebenen Flüssigkeit gemessen wurden.

Um den Einfluss des Abklingens der Emissionsfähigkeit (der Erregung) des nicht eingetauchten Teiles der Probe in der Luftatmosphäre selbst oder in den Flüssigkeitsdämpfen berücksichtigen zu können, wurde immer eine Kontrollprobe benutzt, die in die Flüssigkeit überhaupt nicht eingetaucht wurde.

Zur Untersuchung kamen verschiedene, grösstenteils organische Flüssigkeiten, in deren Molekülen Wasserstoff- und Sauerstoffatome, oder nur Wasserstoffatome, oder weder Wasserstoff- noch Sauerstoffatome eingebaut sind. Der Reinheitsgrad der Flüssigkeiten war „chemisch rein" oder „Pro analisi".

Versuchsergebnisse

1. Mechanische Bearbeitung und danach folgendes Eintauchen in eine Flüssigkeit

Die Flüssigkeiten zeigten verschiedene Einwirkung auf die Abtastkurven der Ph. Ex. Em., je nachdem, ob die Al-Proben vorher mit einer Stahlbürste oberflächlich gerieben oder mit Stahl (Feile, Messerkante) abgeschabt wurden.

a) *Mit Stahlbürste bearbeitete Oberfläche.* In diesem Falle können alle untersuchten Flüssigkeiten in folgende drei Gruppen eingeteilt werden.

1. Gruppe. Zu ihr gehören alle diejenigen Flüssigkeiten, die eine Abnahme der Erregung zur Ph. Ex. Em. im Vergleich zum nichteingetauchten Teil der

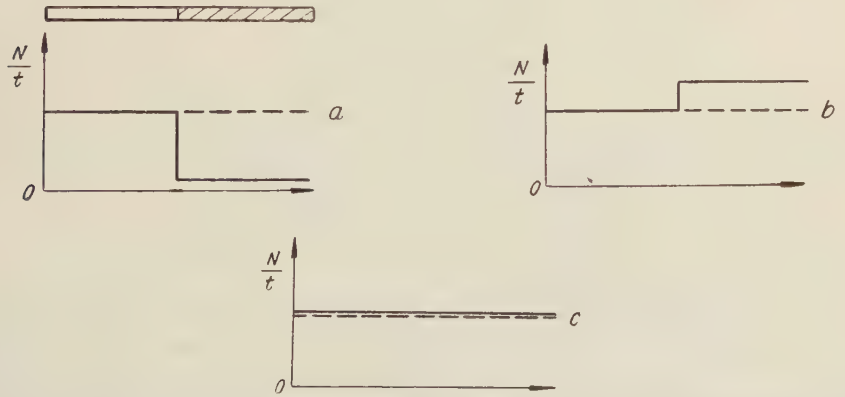

Abb. 2. Ph. Ex. Em. Abtastkurven (schematisch) für Al-Proben, die vorher mit Stahlbürste bearbeitet wurden (— — — —) vor dem Eintauchen, (————————) nach dem Eintauchen in eine der Flüssigkeiten
a) Nach der Einwirkung einer Flüssigkeit der 1 Gruppe (H- sowie O-Atome im Molekül).
b) Nach der Einwirkung einer Flüssikgeit der 2. Gruppe (H- aber keine O-Atome im Molekül).
c) Nach der Einwirkung einer Flüssigkeit der 3. Gruppe (keine H- sowie keine O-Atome im Molekül)
Die Lage der Al-Probe ist über den Abtastkurven angedeutet. Der mit der Flüssigkeit in Berührung kommende Teil ist gestrichelt gezeichnet.

Al-Probe bewirken, wie Wasser (H_2O), Äthylalkohol (C_2H_5OH), Äthyläther ($C_2H_5OC_2H_5$), Essigsäure (CH_3COOH) und Azeton (CH_3COCH_3)*. Siehe Abb. 2a.

2. Gruppe. Zu dieser werden die Flüssigkeiten gerechnet, die den zeitlichen Abfallprozess der Erregung zur Ph. Ex. Em. verlangsamen. Dies wird als eine Zunahme der Erregung zur Ph. Ex. Em. des eingetauchten Teils der Probe im Vergleich zum nichteingetauchten Teil gemessen (siehe Abb. 2b). Hierzu gehören: Benzen (C_6H_6), Toluol ($C_6H_5CH_3$), Chloroform ($CHCL_3$), Trichloräthylen (C_2HCl_3).

3. Gruppe. Zu dieser werden diejenige Flüssigkeiten zugeteilt, die auf die Fähigkeit zur Ph. Ex. Em. keinen Einfluss zu haben scheinen, z. B. Chlorkohlenstoff (CCl_4). Siehe Abb. 2c.

b) *Mit Stahl abgeschabte Oberfläche.* Für alle untersuchten Flüssigkeiten zeigt sich, dass in dem Eintauchsbereich stets eine Abnahme der Intensität der Pb. Ex. Em. im Vergleich zum nichteingetauchten Teil eintritt, wenn die Oberfläche der Al-Probe mit einer Feile oder Messerkante vorher abgeschabt wurde (Abb. 3).

Um festzustellen ob bei den beobachten Erscheinungen die elektrische Leitfähigkeit der Flüssigkeiten keine ausschlaggebende Rolle spielt, wurde die Leitfähigkeit des Azetons mit Hilfe von gelösten KJ um Grössenordnungen geändert. Es konnte jedoch kein deutlicher Einfluss der Leitfähigkeit des Azetons auf seine Löschwirkung gefunden werden, wie dieses nach den Erwägungen von Schaafs (1959) zu erwarten wäre. Wie bekannt, betrachtete Schaafs lokaliesierte, hohe Spannungsgradiente als Ursachen der Emission von Exoelektronen nach mechanischer Erregung.

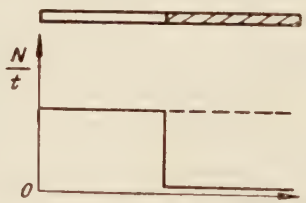

Abb. 3. Ph. Ex. Em. Abtastkurven (schematisch) für Al-Proben, die vorher mit einer Feile oder Messerkante abgeschabt wurden: (– – – – –) vor dem Eintauchen, (——————) nach dem Eintauchen in eine Flüssigkeit irgendeiner der drei Gruppen.

2. Mechanische Bearbeitung, Eintauchen in Flüssigkeiten und danach folgende Erwärmung.

Die Al-Proben wurden wiederum zuerst entweder mit einer Stahlbürste bearbeitet oder mit einer Feile (Messerkante) abgeschabt. Die Proben wurden danach 5 Sekunden lang in einer Flüssigkeit der 2. Gruppe zur Hälfte eingetaucht gehalten, im Luftstrom kalt getrocknet und auf Ph. Ex. Em. Abtastkurven untersucht. Die Proben wurden danach eine Minute lang bei etwa 200°C in der Luftatmosphäre erwärmt. Nach rascher Abkühlung auf Zimmertemperatur wurde die Intensität der Ph. Ex. Em. entlang der Proben als Abtastkurven wiederum gemessen.

* Bei der benutzten Eintauchdauer von 5 Sekunden bewirkt Azeton nur eine verhältnissmässig kleine Abnahme der Erregung zur Ph. Ex. Em.

Auch bei diesem Verfahren wurden wieder qualitativ verschiedene Verläufe der Abtastkurven erhalten, je nachdem ob die Oberfläche zuerst mit einer Stahlbürste bearbeitet oder mit Stahl abgeschabt wurde.

a) *Mit Stahlbürste bearbeitete Oberfläche.* In diesem Fall wird der Kontrast in den Intensitäten der Ph. Ex. Em. zwischen den eingetauchten und nicht eingetauchten Teilen der Proben auch nach der Erwärmung beibehalten. Dieses wird durch die Kurve I (nach dem Eintauchen in der Flüssigkeit der 2. Gruppe) und die Kurve II (nach darauffolgender Erwärmung) in der Abb. 4a illustriert — vergl. auch Abb. 2b. Das Intensitätsniveau der Ph. Ex. Em. wurde entlang der ganzen Probe durch die Erwärmung erniedrigt.

b) *Mit Stahl abgeschabte Oberfläche.* Ein qualitativ anderes Verhalten der Abtastkurve der Ph. Ex. Em. wurde im Falle der Abschabung der Oberfläche mit Stahl (Feile oder Messerkannte) gefunden. Die Abtastkurven zeigten nun eine Umkehrung der Kontraste im Emissionsbild der Proben. Dieses ist schematisch durch die Kurven I und II in der Abb. 4b wiedergegeben. Die Kurve I illustriert den Verlauf der Ph. Ex. Em. nach dem Eintauchen in eine der Flüssigkeiten der 2. Gruppe, die

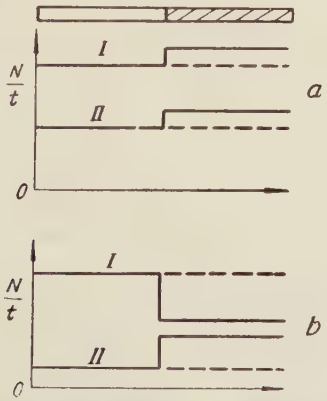

Abb. 4. Ph. Ex. Em. Abtastkurven (schematisch) für Al-Proben, die nach einer mechanischen Bearbeitung der Oberfläche in eine Flüssigkeit der 2. Gruppe eingetaucht (Kurven I) und danach an der Luft bis 200°C erwärmt wurde (Kurven II).
a) Die Al-Oberfläche vorher mit Stahlbürste bearbeitet.
b) Die Al-Oberfläche vorher mit Stahl abgeschabt.

Kurve II illustriert den Verlauf der Abtastkurve gleichen Probe jedoch nach Aufnahme der Kurve I und darauffolgender Erwärmung. Das Intensitätsniveau der Ph. Ex. Em. wurde entlang des nichteingetauchten Teiles der Probe stärker erniedrigt durch die Erwärmung als entlang des eingetauchten Teiles.

3. Einfluss des elektrolytischen Stromes

In weiteren Experimenten wurde der Einfluss des elektrolytischen Stromes auf die Triboerregte Emission orientierungshalber untersucht. Zwei Al-Proben, die vorher mit einer Stahlbürste oberflächlich bearbeitet wurden, wurden als Elektroden in eine schwache KJ-Azetonlösung eingetaucht und einer Gleichstrom-Elektrolyse unter-

worfen. Die Stromdichten betrugen etwa 0.1 mA/cm². Nach einer Minute wurde die Elektrolyse unterbrochen, die Al-Elektroden im „chemisch reinen" Azeton gewaschen und in einem Luftstrom kalt getrocknet. Danach wurden die Abtastkurven der Ph. Ex. Em. entlang der beiden Proben (Elektroden) gemessen.

Es stellte sich heraus, dass an den eingetauchten Teilen der Al-Proben, die während der Elektrolyse als Anoden wirkten, die Erregung zur Ph. Ex. Em. immer stark zurückging im Verleich zur Erregung der nichteingetauchten Teile der Proben. Nach längerer Zeitdauer der Elektrolyse konnte sogar die Erregung zur Ph. Ex. Em. an der Anode völlig ausgelöscht werden, während aus dem nicht eingetauchten Teile der Anode immer noch beträchtliche Emission in Erscheinung trat. Dieses Auslöschen der Erregung an der Anode illustriert die Kurve *A* in Abb. 5a. Die Proben dagegen,

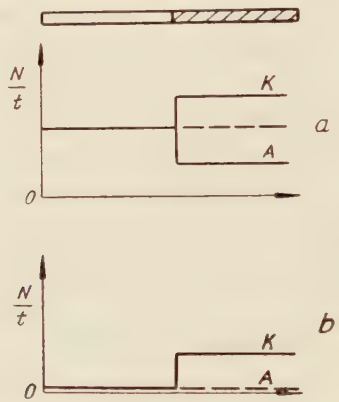

Abb. 5. Ph. Ex. Em. Abtastkurven (schematisch) für Al-Proben, die während einer Elektrolyse in KJ-Azetonlösung als Elektroden wirkten.

a) Al-Proben, die vorher mechanisch bearbeitet wurden und als Kathoden (Kurve *K*) oder als Anoden (Kurve *A*) geschaltet wurden.

b) Al-Proben mit natürlicher Oberflächen — Oxydschicht, die als Kathoden (Kurve *K*) oder als Anoden (Kurve *A*) geschaltet wurden.

die als Kathoden wirkten, zeigten immer eine Erhöhung der Erregung zur Ph. Ex. Em. innerhalb der Teile, die in dem Elektrolyt eingetaucht waren, was schematisch durch die Kurve *K* in Abb. 5a wiedergegeben wurde.

Wenn eine Al-Probe, die keine Erregung zur Ph. Ex. Em. zeigte, als Kathode bei einer Elektrolyse z.B. in eine KJ-Azetonelektrolytlösung eingetaucht wurde, so wurde diese Erregung hervorgerufen. Die Erregung beschränkte sich auf den eingetauchten Bereich der Probe. Die zu einer festgelegten Erregung nötlgen Zeitdauern der Elektrolyse hängen von den Eigenschaften der Deckschicht auf der Al-Probe sowie von den Stromdichten ab.

Die Ph. Ex. Em., die in der Azetonelektrolytlösung an der Kathode elektrolytisch erregt wird, zeigt ähnliche Eigenschaften wie die, die durch eine Abschabung mit Stahl erzielt wird,

Weitere Einzelheiten über elektrolytische Erregbarkeit des Aluminiums sind bei Lewowski (1960) zu finden.

4. Unregelmässigkeiten des Luft-Flüssigkeit Übergangsbereiches

Die untersuchten Al-Proben zeigten ausgeprägte Unregelmässigkeiten in den Abtastkurven Verläufen der Ph. Ex. Em. im Bereich der Luft-Flüssigkeit Eintauchsgrenze. Dieser Grenzbereich mit dem unregelmässigen Verlauf der Abtastkurve ist etwa 1—2 mm breit. Er wurde in dem vorliegenden Bericht übergangen, wird aber bei Gelegenheit näher besprochen.

Diskussion

Die während der Bearbeitung der Al-Oberfläche mit einer Stahlbürste enstandene, sogenannte Beilby-Schicht, besteht vorwiegend aus einem Gemisch von Aluminium und Aluminium-Oxyd (siehe Gomer und Smith 1952). Die unterschiedliche Wirkung der untersuchten Flüssigkeiten auf die Erregung zur Ph. Ex. Em. von Aluminium. das vorher mit einer Stahlbürste bearbeitet wurde, hängt also offensichtlich mit den chemischen Eigenschaften der Flüssigkeiten zusammen (siehe auch Wawrzyniak und Sujak 1960). Beim Kontakt der untersuchten Al-Proben mit der Flüssigkeit kann es also zu einer Oxydation der Aluminium-Elemente und zugleich zu einer damit konkurierenden Reduktion der Oxyd-Elemente der frischen Beilby-Schicht kommen, je nach der zur Verfügung stehenden Menge der aktiven Reaktionspartner: Sauerstoff oder/und Wasserstoff.

Es ist durchaus plausibel anzunehmen, dass wir dabei in erster Phase mit einer katalytischen Zersetzung der Flüssigkeiten an der frisch enstandenen Beilby-Schicht zu tun haben. Die Zersetzungsprodukte können dann in zweiter Phase als aktive Reaktionspartner die Oxydation oder/und die Reduktion bewirken, wie das im Falle der Bildung von H_2O_2 in HzO in Gegenwart von frisch gebrochenem Aluminium und Zink gefunden wurde (Grunberg und Wright 1952, Krause 1958, Churchill 1939).

Es ist bemerkungswert, dass alle untersuchten Flüssigkeiten, die den Abfall der Triboerregung zur Ph. Ex. Em. der Al-Oberfläche (die vorher mit einer Stahlbürste bearbeitet wurde) beschleunigen, in ihren Molekülen Wasserstoff- und Sauerstoffatome enthalten. Die Moleküle der Flüssigkeiten aber, die den zeitlichen Abfall der Triboerregung zur Ph. Ex. Em. verlangsamen, enthalten keine Sauerstoffatome. Demnach also ist es zu erwarten, dass die Moleküle der Flüssigkeiten, die sich in Bezug auf atmosphärische Luft gegenüber der Triboerregung zur Ph. Ex. Em. neutral verhalten, weder Wasserstoff- noch Sauerstoffatome enthalten. Dies ist z.B. an Hand des Chlorkohlenstoffs bestätigt worden. Es ist jedoch zu denken, dass auch die Flüssigkeiten der 3. Gruppe (z.B. Chlorkohlenstoff) das Abklingen der Triboerregung verlangsamen müssen, da der Luftzutritt zu der Oberfläche der Probe während des Kontaktes mit der Flüssigkeit unterbrochen wird. Man darf aber die an der Oberfläche (Beilby-Schicht) adsorbierten Luftreste nicht vergessen. Aus diesem Grunde scheint es verständlich zu sein, dass bei den kurzen Kontaktzeiten (5 Sekunden) kein merklicher

Einfluss des Chlorkohlenstoffs auf die Triboerregung zur Ph. Ex. Em. zu beobachtet wird.

Die kaum merkliche Eigenschaft des Azetons, den Abfall der Triboerregung zu beschleunigen, scheint auf der starken Valenzbildung der Sauerstoffatome in dem Molekül zu beruhen (C = 0). Aus diesen Grunde, wie auch wegen der grossen Abdampfsgeschwindigkeit, kann Azeton zum Abspülen der zur Ph. Ex. Em. erregten Al-Proben erfolgreich benuzt werden (Lewowski 1960).

Wenn eine frische Oberfläche des Aluminiums geschaffen wird, so zeigen sämtliche untersuchte Flüssigkeiten die Tendenz den Abfall der Triboerregung zu beschleunigen (gemessen wird eine Erniedrigung der Intensität der Ph. Ex. Em.). Dieses kommt vor z.B. nach einer vorherigen Abschabung der Oberfläche mit Stahl, und ebenso nach einer voherigen elektrolytischen oder chemischen Reduktion der Oxyddeckschicht. In diesen Fall wird die Tendenz der Flüssigkeiten die Triboerregung zu erniedrigen von uns mit der Bildung von Adsorptions- sowie Oxyddeckschichten erklärt. Damit findet auch die gemessene Erniedrigung der Intensität der Ph. Ex. Em. ihre Erklärung und es wird eine Übereinstimmung erzielt mit den früheren, gut bekannten, klasischen Arbeiten von Suhrmann und seiner Schule über die Rolle der Adsorptionsschichten in den Photoemissionserscheinungen. Zu ähnlichen Feststellungen kamen auch kürzlich Terenin und Willesow (1958) bei den Untersuchungen der Photoemission von Oxyden, sowie Patrick und Choyke (1959) bei den Untersuchungen der Elektronenemission von den *p-n* übergängen in SiC.

Wenn also nach einer Abschabung der Al-Oberfläche der Oxydationsprocess durch das Eintauchen in eine Flüssigkeit der 1. Gruppe frühzeitig beschleunigt wird, so finden wir eine löschende Wirkung der Flüssigkeit wieder (Abb. 3). Diese beruht, unserer Ansicht nach, auf der Bildung einer amorphen Oxydschicht währed des Kontaktes der Oberfläche mit der Flüssigkeit.

Die Adsorptionsdeckschicht, die während des Eintauchens der Al-Probe in die Flüssigkeiten der 2. oder 3. Gruppe ensteht, zeigt zwar keine Oxydationswirkung aber sie kann die Intensität der Ph. Ex. Em. durch die Absorption von Exoelektronen erniedrigen. Diese Deckschicht bildet auch eine Schutzschicht gegen Luftsauerstoff dar. Die letzterwähnte Wirkung der Schutzschicht tritt besonders beim nachträglichen Oxydieren (Erwärmen) der Al-Probe sehr klar hervor. Die Oberfläche des vorher nicht eingetauchten Teiles der Al-Probe oxydiert nämlich schneller bei der leichten Erwärmung als die des eingetauchten Teiles. Dieses führt zur Umkehrung des Intensitätsbildes der Ph. Ex. Em. entlang der Al-Probe (Abb. 4a).

Bei allen diesen Ergebnissen handelt es sich um photoelektrisch emittierte, negativ gelandene Teilchen und nicht um ladungslose Dämpfe, die eine Emission leicht vortäuschen können (Sujak 1958 a, b, 1959 b, Sujak und Bohun 1959).

Es folgt aus den vorgelegten Ergebnissen, dass die photostimulierte Exoelektronenemission einer „frischen" Oberfläche des Aluminiums von der zu unterscheiden ist, die als Folge einer Bildung einer misch-Oxydschicht (Beilby-Schicht) an der Aluminiumoberfläche zum Erscheinen kommt (Sujak und Mader 1958, Bójko, Piróg und Sujak 1958, Sujak 1959a).

Unsere Ergebnisse weisen obendrein auf die Möglichkeit der Heranziehung der Exoelektronenemission zur Untersuchung physikalisch-chemischer Prozesse, die sich an in Flüssigkeiten eingetauchten Elektroden abspielen (Lewowski 1960, Wawrzyniak und Sujak 1960).

LITERATURHINWEISE

Bójko, I., Piróg, M. und Sujak, B., *Z. Naturforsch.*, **13a,** 799 (1958).

Churchill, J. R., *Trans. Electrochem. Soc.*, **76,** 341 (1939).

Gomer, R. und Smith, C. St., *Report of a Conf. in Lake Geneva Wisconsin*, September 1952 "*Structure and Properties of Solid Surface*" University of Chicago Press — Verlag.

Grunberg, L. und Wright, K. H. R., *Nature*, **170,** 456 (1952).

Krauze, A., *Roczniki Chemii*, **32,** 1025 (1958).

Lewowski, T., *Z. Naturforsch.*, **15a,** 90 (1960).

Mader, J. und Sujak, B., *Acta phys. Polon.*, **19,** 179 (1960).

Patrick, L. und Choyke, W. J., *Phys. Rev. Letters*, **2,** 324 (1959).

Schaafs, W., *Z. angew. Phys.*, **11,** 220 (1959).

Sujak, B., *Z. angew. Phys.*, **10,** 531 (1958) a, *Czech. J. Phys.*, **8,** 616 (1958) b, *Phys. Blätt.*, **15,** 209 (1959) a, *Zeszyty Naukowe Uniwersytetu Wrocławskiego*, **3B,** 261 (1959) b.

Sujak, B. und Bohun, A., *Acta phys. Polon.*, **18,** 419 (1959).

Sujak, B. und Mader, J., *Z. Naturforsch.*, **13a,** 55 (1958).

Thomson, N., *Advances in Phys.*, **7** (25), 72 (1958).

Wawrzyniak J., und Sujak, B., *Nature*, **186,** 467 (1960).

Wileşow, F. und Terenin, A., *Naturwissenschaften*, **46,** 167 (1959).

THE COUPLING BETWEEN ELECTRONIC AND NUCLEAR MOTION AND THE RELATIVISTIC EFFECTS IN THE GROUND STATE OF THE H_2 MOLECULE

By W. Kołos and L. Wolniewicz

Department of Electrochemistry, Institute of Physical Chemistry, Polish Academy of Sciences, Warsaw and Department of Theoretical Physics, N. Copernicus University Toruń

(Received July 21, 1960)

The contribution to the binding energy of the hydrogen molecule due to the coupling between nuclear and electronic motion has been calculated. The wave function employed was in the form of an expansion in elliptic coordinates. The most reliable result obtained with a four term expansion is $\Delta D' = -5.1\ \mathrm{cm}^{-1}$. The relativistic corrections calculated with a five term expansion change the binding energy by $\Delta D = -2.4 - E_2\ \mathrm{cm}^{-1}$, where E_2, the classical relativistic correction to the interaction between the electrons, is of the order of $-1\ \mathrm{cm}^{-1}$ or smaller. The calculated corrections added to the accurate non-relativistic result for infinitely heavy nuclei give the theoretical binding energy $D = 38280\ \mathrm{cm}^{-1}$, the experimental value being $D = 38286 \pm 6\ \mathrm{cm}^{-1}$.

1. Introduction

The lowest eigenvalue of the non-relativistic Hamiltonian for the H_2 molecule with fixed nuclei has been computed very accurately by Kołos and Roothaan (1960), but to compare their result with experiment one has to know the magnitude of the contributions to the binding energy due to the motion of the nuclei and to the relativistic effects. Using simple electronic wave functions the first of these corrections have been calculated by Van Vleck (1936) and by Dalgarno and McCarroll (1956), and some of the latter by Ladik (1959). The wave functions employed in these calculations give reasonable values of the total energy of the molecule, however, the results obtained by Dalgarno and McCarroll show that the corrections accounting for the coupling between electronic and nuclear motion are very sensitive to the form of the wave function. It is also well known from atomic calculations that the relativistic corrections are more sensitive to the form of the wave function than the energy itself. It seems therefore desirable to calculate these effects with more accurate wave functions than those used by previous authors.

We have calculated the corrections for nuclear motion and the relativistic ones using for the wave function an expansion in elliptic coordinates. Only 1, 2, 3 and 4 term expansions were employed, however, the method can easily be extended to longer expansions. The relativistic corrections have been computed also with a 5 term wave function in which the fifth term introduced some angular correlation of the electrons. Unfortunately, having no computer, we were not able to calculate the classical relativistic correction due to the interaction between the electrons. However, its magnitude can be estimated, and the detailed method of numerical calculation is given in the Appendix.

2. Energy Corrections Due to the Nuclear-Electronic Coupling

It is well known that in the first approximation the coupling between nuclear and electronic motion changes the molecular energy by[1]

$$E' = E - E_0 = \int \Psi^* H' \Psi \, d\tau_1 \, d\tau_2, \tag{1}$$

where Ψ is the solution of the Schrödinger equation $H_0 \Psi = E_0 \Psi$ with fixed nuclei,

$$H' = -\frac{\hbar^2}{M} \Delta_{\boldsymbol{R}} - \frac{\hbar^2}{4M} (\Delta_{\boldsymbol{r}_1} + \Delta_{\boldsymbol{r}_2} + 2 \nabla_{\boldsymbol{r}_1} \nabla_{\boldsymbol{r}_2}), \tag{2}$$

$\boldsymbol{R}$ denotes the relative coordinate of the nuclei, $\boldsymbol{r}_i$ the position vector of the i-th electron with respect to the centre of R, and M is the proton mass.

The wave function Ψ we assume to be real and given by the expansion

$$\Psi = \sum_i c_i (R) \, \Psi_i (\xi_1, \eta_1, \xi_2, \eta_2 \varphi_1, \varphi_2), \tag{3}$$

where ξ_i, η_i are elliptic coordinates with respect to R and φ_i the azimuthal angle of the i-th electron.

To compute the expectation value of $\Delta_{\boldsymbol{R}}$ using wave function (3) it is convenient to express this operator in terms of ξ_i, η_i, φ_i, R, θ, Φ(θ and Φ are the polar angles of R). After some manipulations one gets

$$\Delta_R = \frac{\partial^2}{\partial R^2} + \frac{2}{R} \frac{\partial}{\partial R} + \frac{1}{R^2} \left(\frac{\partial^2}{\partial \theta^2} + \cot \theta \, \frac{\partial}{\partial \theta} + \frac{1}{\sin^2 \theta} \, \frac{\partial^2}{\partial \Phi^2} \right) +$$

$$+ \Delta (R, \theta, \Phi, \xi_1, \eta_1, \varphi_1) + \Delta (R, \theta, \Phi, \xi_2, \eta_2, \varphi_2) +$$

$$+ \frac{2}{R^2 (\xi_1^2 - \eta_1^2) (\xi_2^2 - \eta_2^2)} \left[\xi_1 (\xi_1^2 - 1) \frac{\partial}{\partial \xi_1} + \eta_1 (1 - \eta_1^2) \frac{\partial}{\partial \eta_1} \right] \times$$

$$\times [\text{similar bracket with } 1 \to 2] + \frac{2}{R^2} \left\{ \frac{\xi_1 \eta_1}{[(\xi_1^2 - 1)(1 - \eta_1^2)]^{1/2}} \frac{\partial}{\partial \varphi_1} + \right.$$

---

[1]) For the derivation and approximations used see Van Vleck (1936), Ta-You Wu and Bhatia (1956), and Dalgarno and McCarroll (1956).

$$+\cos\varphi_1\frac{[(\xi_1^2-1)(1-\eta_1^2)]^{1/2}}{\xi_1^2-\eta_1^2}\left(\eta_1\frac{\partial}{\partial\xi_1}-\xi_1\frac{\partial}{\partial\eta_1}\right)\Bigg\}\{1\to 2\}+\frac{2}{R^2}\Bigg\{\cot\theta\frac{\partial}{\partial\varphi_1}+$$

$$+\frac{\xi_1\eta_1}{[(\xi_1^2-1)(1-\eta_1^2)]^{1/2}}\frac{\partial}{\partial\varphi_1}+\sin\varphi_1\frac{[(\xi_1^2-1)(1-\eta_1^2)]^{1/2}}{\xi_1^2-\eta_1^2}\left(\eta_1\frac{\partial}{\partial\xi_1}-\xi_1\frac{\partial}{\partial\eta_1}\right)\Bigg\}\{1\to 2\},\tag{4}$$

where

$$\Delta(R,\theta,\Phi,\xi,\eta,\varphi)=\frac{\xi^2+\eta^2-1}{R^2(\xi^2-\eta^2)}\left\{\frac{\partial}{\partial\xi}(\xi^2-1)\frac{\partial}{\partial\xi}+\frac{\partial}{\partial\eta}(1-\eta^2)\frac{\partial}{\partial\eta}+\right.$$

$$\left.+\left(\frac{1}{\xi^2-1}-\frac{1}{1-\eta^2}\right)\frac{\partial^2}{\partial\varphi^2}\right\}-\frac{2}{R^2(\xi^2-\eta^2)}\left\{\xi(\xi^2-1)\frac{\partial}{\partial\xi}+\eta(1-\eta^2)\frac{\partial}{\partial\eta}\right\}\times$$

$$\times\left(1+R\frac{\partial}{\partial R}\right)+\frac{1}{R^2}\left\{\frac{1}{\sin^2\theta}\frac{\partial}{\partial\varphi}-2\frac{\cot\theta}{\sin\theta}\frac{\partial}{\partial\Phi}-2\frac{\partial}{\partial\varphi}\right\}\frac{\partial}{\partial\varphi}+$$

$$+\frac{2\xi\eta}{R^2[(\xi^2-1)(1-\eta^2)]^{1/2}}\left\{\sin\varphi\frac{\partial}{\partial\theta}-\frac{\cos\varphi}{\sin\theta}\frac{\partial}{\partial\Phi}+\cos\varphi\cot\theta\frac{\partial}{\partial\varphi}\right\}\frac{\partial}{\partial\varphi}-$$

$$-\frac{2[(\xi^2-1)(1-\eta^2)]^{1/2}}{R^2(\xi^2-\eta^2)}\left\{\cos\varphi\frac{\partial}{\partial\theta}+\frac{\sin\varphi}{\sin\theta}\frac{\partial}{\partial\Phi}-\sin\varphi\cot\theta\frac{\partial}{\partial\varphi}\right\}\left(\eta\frac{\partial}{\partial\xi}-\xi\frac{\partial}{\partial\eta}\right).$$

If we restrict ourselves to wave functions of the form

$$\Psi=\sum c_k^p(R)\,g_k(\xi_1,\eta_1,\xi_2,\eta_2)\,\chi^p(\xi_1,\eta_1,\xi_2,\eta_2,\varphi)\tag{5}$$

where $\varphi=\varphi_1-\varphi_2$ and $R^p\chi^p$ is a homogeneous function of the p-th degree of $\boldsymbol{r}_i$ only, then the expression (4) can be reduced as follows:

From the definition of χ^p we have[2]

$$\nabla_{\boldsymbol{R}}R^p\chi^p=0,\tag{6}$$

and

$$\int\Psi\,\Delta_{\boldsymbol{R}}\Psi\,d\tau_1\,d\tau_2=\sum_{k,p}\int\Psi R^p\chi^p\,\Delta_{\boldsymbol{R}}R^{-p}c_k^p g_k\,d\tau_1\,d\tau_2.\tag{7}$$

Now, in (7) we can drop all terms containing derivatives with respect to any angle, and due to the symmetry $\chi^p(\varphi+2\pi)=\chi^p(\varphi)$ all terms linear in $\cos\varphi_i$ or $\sin\varphi_i$. If in addition we take into account the fact that the wave function is symmetric in the coordinates of the two electrons, we can replace $\Delta_{\boldsymbol{R}}$ by $\Delta'_{\boldsymbol{R}}$, were

$$\Delta'_{\boldsymbol{R}}=\frac{\partial^2}{\partial R^2}+\frac{2}{R}\frac{\partial}{\partial R}+\frac{2(\xi_1^2+\eta_1^2-1)}{R^2(\xi_1^2-\eta_1^2)}\left\{\frac{\partial}{\partial\xi_1}(\xi_1^2-1)\frac{\partial}{\partial\xi_1}+\frac{\partial}{\partial\eta_1}(1-\eta_1^2)\frac{\partial}{\partial\eta_1}\right\}-$$

$$-\frac{4}{R^2(\xi_1^2-\eta_1^2)}\left\{\xi_1(\xi_1^2-1)\frac{\partial}{\partial\xi_1}+\eta_1(1-\eta_1^2)\frac{\partial}{\partial\eta_1}\right\}\left(1+R\frac{\partial}{\partial R}\right)+$$

---

[2]) $\nabla_{\boldsymbol{R}}$ means differentiation with respect to $\boldsymbol{R}$ with $\boldsymbol{r}_i$ kept constant.

$$+\frac{2}{R^2(\xi_1^2-\eta_1^2)(\xi_2^2-\eta_2^2)}\left[\xi_1^2(\xi_1^2-1)\frac{\partial}{\partial\xi_1}+\eta_1(1-\eta_1^2)\frac{\partial}{\partial\eta_1}\right]\left[\xi_2(\xi_2^2-1)\frac{\partial}{\partial\xi_2}+\right.$$

$$\left.+\eta_2(1-\eta_2^2)\frac{\partial}{\partial\eta_2}\right]+\frac{2}{R^2}[(\xi_1^2-1)(1-\eta_1^2)(\xi_2^2-1)(1-\eta_2^2)]^{1/2}\times$$

$$\times\cos(\varphi_1-\varphi_2)\left[\eta_1\frac{\partial}{\partial\xi_1}-\xi_1\frac{\partial}{\partial\eta_1}\right]\left[\eta_2\frac{\partial}{\partial\xi_2}-\xi_2\frac{\partial}{\partial\eta_2}\right]. \tag{8}$$

Finally, to compute (7), one has to know the derivative

$$\frac{d\Psi}{dR}=\sum\frac{dc_k}{dR}\Psi_k(\xi_1,\eta_1,\xi_2,\eta_2,\varphi_1,\varphi_2), \tag{9}$$

which can be found in the following way. Let us denote

$$H_{ik}=\int\Psi_i H_0\Psi_k,\quad V_{ik}=\int\Psi_i V\Psi_k,\quad S_{ik}=\int\Psi_i\Psi_k. \tag{10}$$

For any R the coefficients $c_k(R)$ satisfy the set of equations

$$\sum_k c_k(R)[H_{ik}-E_0 S_{ik}]=0.$$

$$\sum_{i,k}c_i c_k S_{ik}=1. \tag{11}$$

A differentiation of (11) gives than after simple manipulations

$$\sum_k[H_{ik}-E_0 S_{ik}]\frac{dc_k}{dR}=\sum_k\left[\frac{2H_{ik}-V_{ik}}{R}+\frac{dE_0}{dR}S_{ik}\right]c_k,$$

$$\sum_{i,k}c_i\frac{dc_k}{dR}S_{ik}=-\frac{3}{R},$$

$$\frac{dE_0}{dR}=-\frac{2E_0-V}{R}, \tag{12}$$

and by solving this set of equations one can easily find the derivative dc_k/dR. Similarly, by differentiation of (12), it is possible to get any higher derivative of Ψ with respect to R.

Let us now define

$$E_3'=-\frac{\hbar^2}{2M}\int\Psi\nabla_{r_1}\nabla_{r_2}\Psi\,d\tau_1\,d\tau_2$$

A convenient expression for the calculation of E_3' we shall give under the assumption

$$g_n=g_{klk'l'}=e^{-\alpha(\xi_1+\xi_2)}\xi_1^k\eta_1^l\xi_2^{k'}\eta_2^{l'}$$

and for two special functions

$$\chi^p = \varrho^p \equiv \left(\frac{2\,r_{12}}{R}\right)^p, \tag{13}$$

and

$$\chi^{2p} = \Phi^p \equiv [(\xi_1^2 - 1)\,(1 - \eta_1^2)\,(\xi_2^2 - 1)\,(1 - \eta_2^2)]^{\frac{p}{2}} \cos p\,(\varphi_1 - \varphi_2)\,. \tag{14}$$

Due to the symmetry we have

$$E_3' = \sum a_{klk'l'}^p \int \Psi \{\chi^p \nabla_{r_1} \nabla_{r_2} g_n + 2\,(\nabla_{r_1} \chi^p)\,(\nabla_{r_2} g_n) + g_n \nabla_{r_1} \nabla_{r_2} \chi^p\}\, d\tau_1\, d\tau_2\,,$$

So, using the relations

$$\nabla_{r_1} \nabla_{r_2} g_{klk'l'} = \frac{2 g_{klk'l'}}{R^2\,(\xi_1^2 - \eta_1^2)\,(\xi_2^2 - \eta_2^2)}\,(\xi_1^2 + \xi_2^2 + \eta_1^2 + \eta_2^2 - 2 - \varrho^2)\,(\alpha\,\xi_1 -$$

$$- k + l)\,(\alpha\xi_2 - k' + l') +$$

$$+ \frac{4 g_{k-1,\,l-1,\,k'-1,\,l'-1}}{R^2\,(\xi_1^2 - \eta_1^2)\,(\xi_2^2 - \eta_2^2)}\,\{(\alpha\eta_1^2\,\xi_1 - k\eta_1^2 + l\xi_1^2)\,(\alpha\eta_2^2\,\xi_2 - k'\,\eta_2^2 + l'\xi_2^2) +$$

$$+ \xi_1^2\,\eta_1^2\,(\alpha\xi_1 - k + l)\,(-\alpha\eta_2^2\,\xi_2 + k'\,\eta_2^2 - l'\xi_2^2) +$$

$$+ \xi_2^2\,\eta_2^2\,(\alpha\xi_2 - k' + l')\,(-\alpha\eta_1^2\,\xi_1 + k\eta_1^2 - l\xi_1^2)\},$$

$$\nabla_{r_1} \varrho^p \nabla_{r_2} g_{klk'l'} = \frac{4p\varrho^{p-2}}{R^2\,(\xi_2^2 - \eta_2^2)} \left\{\frac{1}{2}\,(\varrho^2 + \xi_2^2 + \eta_2^2 - \xi_1^2 - \eta_1^2)\,(\alpha\xi_2 - k' + l') +\right.$$

$$\left. + (\xi_2\,\eta_2 - \xi_1\,\eta_1)\left(-\alpha\eta_2 + k'\,\frac{\eta_2}{\xi_2} - l'\,\frac{\xi_2}{\eta_2}\right)\right\} g_{klk'l'},$$

$$\nabla_{r_1} \nabla_{r_2} \varrho^p = -\,\frac{4}{R^2}\,p\,(p+1)\,\varrho^{p-2},$$

$$\nabla_{r_1} \Phi^p \nabla_{r_2} g_{klk'l'} = \frac{4p\,(\xi_2^2 - 1)\,(1 - \eta_2^2)}{R^2\,(\xi_2^2 - \eta_2^2)}\,\Phi^{p-1} \left(\xi_2\,\frac{\partial}{\partial\,\xi_2} - \eta_2\,\frac{\partial}{\partial\eta_2}\right) g_{klk'l'},$$

$$\nabla_{r_1} \nabla_{r_2} \Phi^p = \frac{8p^2}{R^2}\,\Phi^{p-1},$$

in the case (13) we can express E_3' in terms of integrals

$$\int e^{-2\alpha(\xi_1 + \xi_2)}\,\varrho^s\,\frac{\xi_1^k\,\eta_1^l\,\xi_2^{k'}\,\eta_2^{l'}}{(\xi_1^2 - \eta_1^2)\,(\xi_2^2 - \eta_2^2)}\,d\tau_1\,d\tau_2\,,$$

where $s \geqslant -1$ and $k,\ l,\ k',\ l' \geqslant 0$, and in the case (14) in terms of

$$\int e^{-2\alpha(\xi_1+\xi_2)}\,\xi_1^k\,\eta_1^l\,\xi_2^{k'}\,\eta_2^{l'}\,d\xi_1\,d\xi_2\,d\eta_1\,d\eta_2\,.$$

The last conclusion follows from the orthogonality of Φ^p functions with different p indices, and from the identity

$$\varrho^2 = \xi_1^2 + \eta_1^2 + \xi_2^2 + \eta_2^2 - 2 - 2\,\xi_1\,\xi_2\,\eta_1\,\eta_2 - 2\,\Phi^1\,.$$

3. The Relativistic Corrections

For the calculation of the relativistic correction E_{rel} we have used the Hamiltonian given by Bethe and Salpeter (1957). So, in their notation

$$E_{rel} = \int \Psi H_{rel} \Psi\, d\tau = E_1 + E_2 + E_3 + E_4 + E_5 + E_6\,. \tag{15}$$

For the ground state of the H_2 molecule E_3 and E_6 are zero, and if use is made of the symmetry of Ψ the non-vanishing contributions to E_{rel} read

$$E_1 = -\frac{\hbar^4}{4m^3c^2}\int (\Delta_{r_1}\Psi)^2\,d\tau_1\,d\tau_2\,,$$

$$E_2 = -\frac{e^2}{2(mc)^2}\int \Psi\,\frac{1}{r_{12}}\left[\boldsymbol{p}_1\cdot\boldsymbol{p}_2 + \frac{\boldsymbol{r}_{12}\,(\boldsymbol{r}_{12}\,\boldsymbol{p}_1)\,\boldsymbol{p}_2}{r_{12}^2}\right]\Psi\,d\tau_1\,d\tau_2\,,$$

$$E_4 = \frac{4\pi^2 e^2\hbar^2}{(2mc)^2}\int \Psi\Psi\,[2\delta(\boldsymbol{r}_{1a}) - \delta(\boldsymbol{r}_{12})]\,d\tau_1\,d\tau_2\,,$$

$$E_5 = \frac{8\pi e^2\hbar^2}{(2mc)^2}\int \Psi\Psi\,\delta(\boldsymbol{r}_{12})\,d\tau_1\,d\tau_2\,, \tag{16}$$

where $\boldsymbol{p}_i$ is the momentum operator of the i-th electron, and $\boldsymbol{r}_{1a}$ the position vector of the electron denoted by 1 with respect to the nucleus a.

The calculation of E_4 and E_5 is straightforward. If the function (13) is used in the calculation of E_1 it gives integrals with r_{12}^{-2} in the integrand. We have not been able to find a method of integration in this case. If we use the function (14) the integration in E_1 can be performed in the following way. A typical integral for the computation of E_1 reads

$$\int (\Delta_{r_1} g_i \Phi^p)\,(\Delta_{r_1} g_j \Phi^{p'})\,d\tau_1\,d\tau_2 \tag{17}$$

As a consequence of

$$\Delta_{r_1}\Phi^p = 0,$$

$$(\nabla_{r_1}\Phi^p)\,(\nabla_{r_1} g_j) = \frac{4p}{R^2(\xi_1^2 - \eta_1^2)}\,\Phi^p\left(\xi_1\frac{\partial}{\partial\xi_1} - \eta_1\frac{\partial}{\partial\eta_1}\right) g_j\,,$$

after integration over φ, (17) vanishes unless $p = p'$. Now it is clear that (17) is a sum of integrals of the type

$$\int e^{-2\alpha(\xi_1+\xi_2)}\, \xi_1^k\, \eta_1^l\, \xi_2^{k'}\, \eta_2^{l'}\, (\xi_1^2 - \eta_1^2)^{-1}\, (\xi_2^2 - \eta_2^2)\, d\xi_1\, d\xi_2\, d\eta_1\, d\eta_2 .$$

The ξ_2, η_2 integration is trivial, and the integration over η_1 leads to two types of integrals

$$\int_1^\infty e^{-2\alpha\xi_1}\, \xi_1^n\, d\xi_1, \quad n \geqslant 0,$$

$$\int_1^\infty e^{-2\alpha\xi_1}\, \xi_1^s \lg \frac{\xi_1 - 1}{\xi_1 + 1}\, d\xi_1, \quad s \geqslant -1,$$

which can be expressed in terms of $Ei\,(-2\alpha)$ if $s \neq -1$. In the case of $s = -1$ one has to perform the integration numerically.

4. *Numerical Results*

The wave function we employed was of the form

$$\Psi = \frac{1}{2\pi}\, e^{-\alpha(\xi_1+\xi_2)} \sum_{i=1}^{n} c_i(R)\, g_i, \quad n = 1, 2, 3, 4, 5, \tag{18}$$

where

$$g_1 = 2, \quad g_2 = \eta_1^2 + \eta_2^2, \quad g_3 = 2\eta_1\eta_2,$$

$$g_4 = \xi_1 + \xi_2, \quad g_5 = 2\,[(\xi_1^2 - 1)\,(1 - \eta_1^2)\,(\xi_2^2 - 1)\,(1 - \eta_2^2)]^{1/2} \cos(\varphi_1 - \varphi_2).$$

All calculations have been carried out for the internuclear distance $R = 1.4$ au, and using $\alpha = 0.95$. The coefficients c_i (R), and E_0, i.e. the expectation values of H_0 (in au), as well as the corresponding binding energies D (in eV) are given in Table I.

Table I

n	E_0 (au)	D (eV)	c_1	c_2	c_3	c_4	c_5
1	−1.08612	2.343	4.07284				
2	−1.11544	3.141	3.45343	2.03585			
3	−1.13560	3.690	3.38893	2.16629	−1.47897		
4	−1.15165	4.126	1.73628	2.00821	−1.38824	0.82506	
5	−1.16081	4.376	1.70621	1.95257	−1.35017	0.84280	−0.16518

The corrections due to the coupling between nuclear and electronic motion have been computed with four wave functions ($n = 1, 2, 3, 4$). They are presented in Table II in which the first column gives the number of terms in the wave function, the next three give

$$E_1' = -\frac{\hbar^2}{M}\int \Psi \Delta_R \Psi d\tau_1 d\tau_2,$$

$$E_2' = -\frac{\hbar^2}{4M}\int \Psi (\Delta_{r_1} + \Delta_{r_2}) \Psi d\tau_1 d\tau_2,$$

$$E_3' = -\frac{\hbar^2}{2M}\int \Psi \nabla_{r_1} \nabla_{r_2} \Psi d\tau_1 d\tau_2$$

in au/M (= 119.47 cm^{-1}), and the last one $E' = E_1' + E_2' + E_3'$ in cm^{-1}.

Table II

n	E_1'	E_2'	E_3'	E' (cm^{-1})
1	0.9822	0.6508	0	195.1
2	1.1640	0.6790	0	220.2
3	1.2188	0.6942	0.0270	231.8
4	0.4401	0.5831	0.0198	124.6
$R = 0$	0	1.4519	0.0401	178.3
$R = \infty$	0.5	0.5	0	119.5

Although the final corrections do not show any convergence the result obtained with the 4 term wave function seems to be the most reliable. In this case the second term, E_2, which is proportional to the kinetic energy of the electrons, differs only slightly from the accurate value 0.5875. Van Vleck (1936) employing the Wang wave function obtained a smaller correction E' = 114 cm^{-1}, and the Heitler London wave function with $\zeta = 1$ in the atomic orbitals (Dalgarno and McCarroll 1956) gave a still smaller value.

In the last two lines of Table II accurate values of the corrections for infinitely separated and coalesced nuclei are given. By comparing our 4 term result with that for $R = \infty$ we see that the coupling between electronic and nuclear motion gives a *negative* contribution to the binding energy $\Delta D' = -5.1$ cm^{-1}, whereas Van Vleck obtained a positive value $\Delta D' = +5$ cm^{-1}.

The relativistic corrections have been computed with all five wave functions (18). The last one accounts for 92% of the binding energy. The results in cm^{-1} $\left(\frac{\alpha^2}{2}\text{au} = 5.844\text{ cm}^{-1}\right)$ are presented in Table III.

Table III

n	E_1	E_4	E_5	E'' (cm^{-1})
1	− 15.3	12.2	4.2	1.1
2	− 22.8	17.6	4.1	− 1.1
3	− 24.5	18.7	3.2	− 2.6
4	− 18.0	15.2	2.4	− 0.4
5	− 17.7	15.0	2.2	− 0.5
Ladik	− 46.3	15.5	1.9	−28.9
$R = 0$	−158.1	129.0	7.8	−21.3
$R = \infty$	− 14.6	11.7	0	− 2.9

In the last column of the Table the sum $E'' = E_1 + E_4 + E_5 = E_{\text{rel}} - E_2$ is given. Accurate values for $R = 0$ and $R = \infty$ are also shown in the Table. As mentioned in the Introduction we were not able to calculate E_2. This correction, being due to the retardation of the electromagnetic field produced by an electron, vanishes for $R = \infty$ and has the value $E_2 = -1.64\ \text{cm}^{-1}$ for $R = 0$. For $R = R_e$ it is probably of the order of -1 or smaller in absolute value. Ladik's (1959) results obtained with the Wang wave function are also given in Table III. The origin of the discrepancy between his result for E_1 and ours is not clear[3].

From Table III we see that the relativistic corrections give a *negative* contribution to the binding energy $\Delta D = -2.4 - E_2\ \text{cm}^{-1}$. Thus, according to our calculation, the relativistic effects and the coupling between electronic and nuclear motion *decrease* the theoretical binding energy $D_{\text{th}} = 38287\ \text{cm}^{-1}$ by 6—7 cm^{-1}. The final result is still in agreement with the experimental value $D_{\text{exp}} = 38286 \pm 6\ \text{cm}^{-1}$, however, more accurate calculation of the corrections is clearly desirable.

Appendix

Now we shall outline a method convenient for the calculation of E_2 with a wave function of the form (5)

$$\Psi = e^{-\alpha(\xi_1+\xi_2)} \sum_{k,p\geqslant 0} c_k^p\, g_k\,(\xi_1, \eta_1, \xi_2, \eta_2)\, \Phi^p, \tag{A1}$$

where g_k are polynomials, and

$$\Phi^p = \chi^{2p} = A^p \cos p\,(\varphi_1 - \varphi_2),$$

$$A = [(\xi_1^2 - 1)\,(1 - \eta_1^2)\,(\xi_2^2 - 1)\,(1 - \eta_2^2)]^{\frac{1}{2}}.$$

[3]) In Ladik's paper E_{rel} is decomposed in a slightly different way ($E_{1L} = E_1 + E_4$, $E_{6L} = E_5$, $E'_{1L} = E_4 + \frac{1}{2} E_5$, $E'_{1L} = E_1$, where E_{iL} means E_i in Ladik's paper), and the relativistic Hamiltonian he uses is different from ours, E_4 being counted twice. This, however, does not influence the results given in Table III.

It can be shown that E_2 is expressible in terms of the well known W_τ^ν integrals (Kotani et al. 1955), and of the integral

$$I = \int \Psi \frac{1}{\varrho^3} U d\tau_1 d\tau_2, \tag{A2}$$

where

$$\varrho = \frac{2r_{12}}{R}, \qquad U = \frac{\exp[-\alpha(\xi_1+\xi_2)]}{(\xi_1^2-\eta_1^2)(\xi_2^2-\eta_2^2)} \{O_1 u_1 + O_2 u_2\}.$$

The functions u_j have the form

$$u_j = \sum a^p_{iklm} \xi_1^i \eta_1^k \xi_2^l \eta_2^m \Phi^p,$$

and[4]

$$O_1 = \xi_1\eta_1 - \xi_2\eta_2, \qquad O_2 = \xi_1^2 + \eta_1^2 - \xi_2^2 - \eta_2^2.$$

The integral (A2) can then be expressed in terms of

$$I^i_{pp'kk'll'} = \int e^{-2\alpha(\xi_1+\xi_2)} \xi_1^k \eta_1^l \xi_2^{k'} \eta_2^{l'} \Phi^p \Phi^{p'} \frac{O_i}{\varrho^3} d\xi_1 \ldots dq_2 \tag{A3}$$

and due to the fact that

$$\Phi^p \Phi^{p'} = \tfrac{1}{2}\Phi^{p+p'} + \tfrac{1}{2} A^{2p'} \Phi^{p-p'}, \qquad p \geqslant p', \tag{A4}$$

also in terms of

$$\bar{I}^i_{pskk'll'} = \int e^{-2\alpha(\xi_1+\xi_2)} \xi_1^k \eta_1^l \xi_2^{k'} \eta_2^{l'} A^{2s} \Phi^p \frac{O_i}{\varrho^3} d\xi_1 \ldots dq_2. \tag{A5}$$

Now we can expand ϱ^{-3} in a series. We have obviously

$$\varrho^{-3} = -\frac{1}{A \sin\varphi} \frac{d}{d\varphi} \varrho^{-1}, \tag{A6}$$

where $\varphi = \varphi_1 - \varphi_2$.
By making use of the well known Neumann's expansion for ϱ^{-1} one gets

$$\varrho^{-3} = \frac{1}{A} \sum_{\tau=0}^{\infty} \sum_{n=1}^{\tau} n D_{\tau n} Q_\tau^n(\xi_+) P_\tau^n(\xi_-) P_\tau^n(\eta_1) P_\tau^n(\eta_2) \frac{\sin n\varphi}{\sin\varphi}, \tag{A7}$$

with

$$D_{\tau n} = (-1)^n 2(2\tau+1) \left[\frac{(\tau-n)!}{(\tau+n)!}\right]^2.$$

---

[4]) Note that $O_1 = \frac{2}{R}(z_1 - z_2)$, $O_2 = \frac{4}{R^2}(r_1^2 - r_2^2)$, hence (A2) is finite.

The substitution of (A7) into (A5), after integration over φ_1 an φ_2, gives

$$\bar{I}^{i}_{pskk'll'} = (2\pi)^2 \sum_{\tau=0}^{\infty} \sum_{n=p+1}^{\tau} \frac{n}{2} \left|(-1)^{p+1} + (-1)^n\right| L^{n}_{\tau,ijps} \tag{A8}$$

where

$$L^{n}_{\tau,ijps} = D_{\tau n} \int O_i \, e^{-2\alpha(\xi_1+\xi_2)} \, \xi_1^k \, \eta_1^l \, \xi_2^{k'} \, \eta_2^{l'} \, A^{2s+p-1} \, Q^n_\tau(\xi_+) \times$$
$$\times \, P^n_\tau(\xi_-) \, P^n_\tau(\eta_1) \, P^n_\tau(\eta_2) \, d\xi_1 \ldots d\eta_2, \tag{A9}$$

and j is an abbreviation for $kk'll'$.
Remembering the definition of O_i one sees that (A9) is a combination of integrals of the type

$$J^{n}_{\tau,sj} = D_{\tau n} \int e^{-2\alpha(\xi_1+\xi_2)} \, \xi_1^k \, \eta_1^l \, \xi_2^{k'} \, \eta_2^{l'} \, A^s \, Q^n_\tau(\xi_+) \, P^n_\tau(\xi_-) \, P^n_\tau(\eta_1) \, P^n_\tau(\eta_2) \, d\xi_1 \ldots d\eta_2. \tag{A10}$$

From (A9) it is clear that $s \geqslant -1$. So if we remember that $\xi_+ \geqslant \xi_-$ and $n \geqslant 1$ we can easily show that (A10) does not diverge[5]
Let us now define

$$K^{n}_{\tau,sl} = \int_{-1}^{1} \eta^l \, (1-\eta^2)^{\frac{s}{2}} \, P^n_\tau(\eta) \, d\eta. \tag{A11}$$

With this definition (A10) reads

$$J^{n}_{\tau,sj} = D_{\tau n} \, K^{n}_{\tau,sl} \, K^{n}_{\tau,sl'} \int e^{-2\alpha(\xi_1+\xi_2)} \, \xi_1^k \, \xi_2^{k'} \, (\xi_1^2-1)^{\frac{s}{2}} \, (\xi_2^2-1)^{\frac{s}{2}} \, Q^n_\tau(\xi_+) \times$$
$$\times \, P^n_\tau(\xi_-) \, d\xi_1 \, d\xi_2, \tag{A12}$$

and making use of the generalized Ruedenberg's formula given by Harris (1960) we have finally

$$J^{n}_{\tau,sj} = 2\,(2\tau+1) \, K^{n}_{\tau,sl} \, K^{n}_{\tau,sl'} \int_{1}^{\infty} G^{n}_{\tau sk}(x) \, G^{n}_{\tau sk'}(x) \, dx, \tag{A13}$$

where

$$G^{n}_{\tau sk} = [(x^2-1)^{\frac{1}{2}} \, P^n_\tau(x)]^{-1} \int_{1}^{x} e^{-2\alpha\xi} \, \xi^k \, (\xi^2-1)^{\frac{s}{2}} \, P^n_\tau(\xi) \, d\xi.$$

It is easy to show that

$$\lim_{x \to 1} G^{n}_{\tau sk}(x) = \begin{cases} \dfrac{\exp(-2\alpha)}{n+1} & \text{if } s = -1, \\ 0 & \text{if } s > -1. \end{cases} \tag{A14}$$

From (A14) it follows that the product $G^{n}_{\tau sk} \, G^{n}_{\tau sk'}$ has no poles and (A13) can be simply computed by numerical integration.

---

[5]) If $s \geqslant n$ then (A10) is expressible in terms of the W^{v}_{τ} integrals.

REFERENCES

Bethe, H. A. and Salpeter, E. E., *Encyclopedia of Physics*, **35/1**, 267 (1957).
Dalgarno, A. and McCarroll, R., *Proc. Roy. Soc.*, **237**, 383 (1956).
Harris, F. E., *J. chem. Phys.* **32**, 3 (1960).
Kołos, W. and Roothaan, C. C. J., *Rev. mod. Phys.*, (1960).
Kotani, M., Amemiya, A., Ishiguro, E., Kimura, T., *Table of Molecular Integrals*, Tokyo (1955).
Ladik, J., *Acta phys. Hungar.*, **10**, 271 (1959).
Van Vleck, J. H., *J. chem. Phys.*, **4**, 327 (1936).
Wu, Ta-You and Bhatia, A. B., *J. chem. Phys.*, **24**, 48 (1956).

FIRST INVESTIGATION ON CLOUDS OVER BRITISH ISLES USING AN AIRCRAFT

By Józef Mazur

Physics Department of the University
and
Low Temperature Laboratory of the Institute of Physics Polish Academy of Sciences,
Wrocław, Poland

(Received August 25, 1960)

The danger to aircraft of ice formations was given rise to a number of experiments in which the ice formation is produced artificially under controlled conditions of temperature, airspeed, size and number of suspended water particles.

The applications of the results of such experiments depend on information about the number and size distribution of water particles in natural clouds.

In order to get such necessary information the author on the behalf of the Air Ministry, Meteorological Research Committee, carried out during the war the investigations in all types of clouds over the British Isles and fogs (Fog Investigation and Dispersal Operation better known as FIDO).

Introduction

Cloud is a colloidal suspension of water in air and has been described by Wigand and Schmauss (1929) as an aerosol. The suspended water is in the form of liquid droplets, ice crystals or mixture of droplets and crystals. Water particles in clouds are often supercooled in a liquid state at temperatures far below freezing point, sometimes at $-50°$ C. (Perrie, 1950).

The danger to aircraft of ice formation has given rise to a number of experiments, in which the ice formation is produced artificially under controlled conditions of temperature, airspeed, size and number of suspended particles. The application of the results of such experiments depends on information about the number and size distribution of water particles in natural clouds. In 1941—42 the writer prepared for the Director, Meteorological Office, Air Ministry, London, a memorandum, summarizing the existing knowledge on this subject and indicating the lines, on which further investigation was needed (Mazur, 1941, 1942). As a first step it was necessary to devise an apparatus for sampling the water droplets, to develop a technique and begin observations. It is worth to mention that the first systematic study of cloud drops was carried out by Bricard (1939, 1940) on the Puy de Dôme and later on the Pic-du-Midi.

General description of the Apparatus

The apparatus, known later as the Aircraft Impactor, was conceived on the lines of the Porton Impactor (Davies, 1942). The latter consisted of a wood and metal holder for a glass plate. The wooden front is "streamlined" and has a slot through which the natural wind passes, thus playing on the surface of the glass plate clamped at right angles to the outlet of the slot. The air stream impinging upon the plate escapes round two sides of the plate. The air has to turn through a right angle, and the particles having sufficient kinetic energy are unable to turn the corner and so strike and adhere to the plate. Smaller drops will be more or less deviated but all drops greater than some critical size will strike the slide.

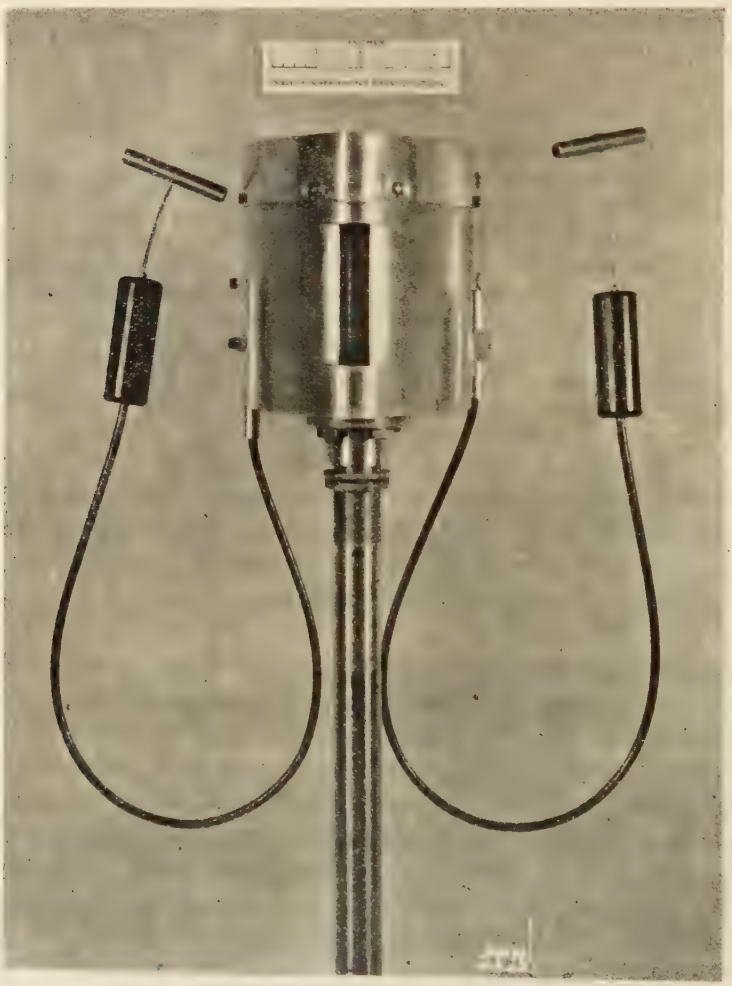

Fig. 1. Crown copyright reserved. Reproduced with the permission of the Controller, H.M.S.O. Front view of Aircraft Impactor showing front shuter open.

The Aircraft Impactor

The first type of aircraft impactor, made in the Instruments Branch of the Meteorological Office at Stonehouse, retained the shape of the Porton impactor but differed in regard to the shutters. Those consisted of two coaxial semicylindrical cases, arranged to rotate in opposite directions and each provided with a slot parallel to the axis. By suitable setting of a spring controlling the mechanism the slots could be brought together to give the correct exposure.

After trials of this first model in a wind tunnel and on aircraft an improved impactor was made. The body was cut from a solid aluminium block and was therefore very strong, the slot was shortened and the sampling plate reduced to half the size of a quarter plate (Mazur, 1943).

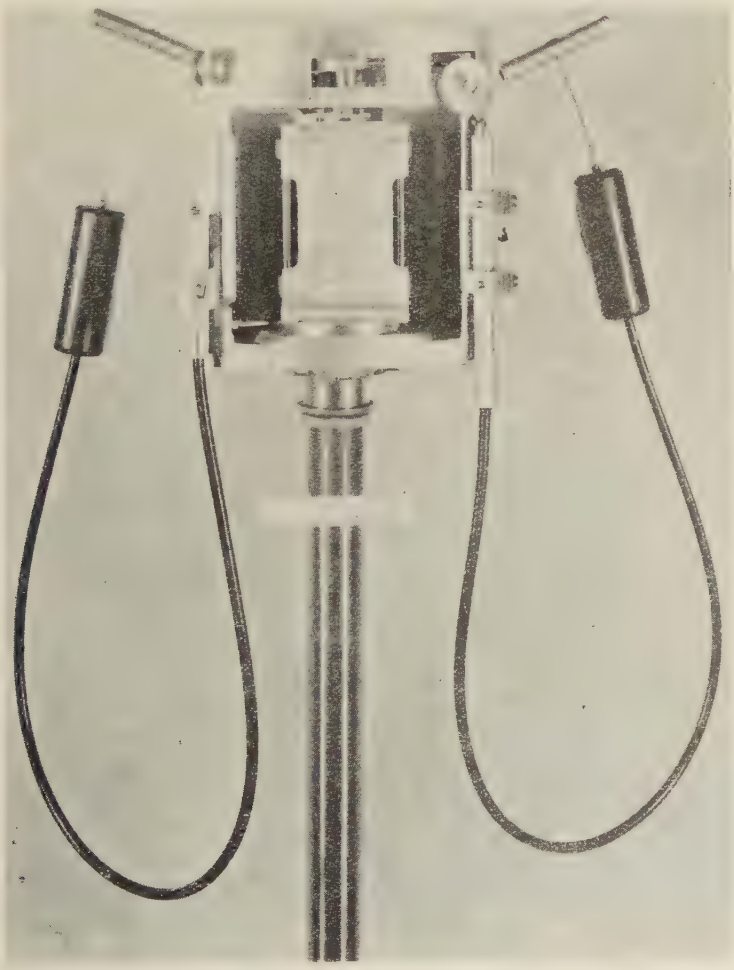

Fig. 2. Crown copyright reserved. Reproduced with the permission of the Controller, H.M.S.O. Back of the Aircraft Impactor showing plate holder swung round to position for changing plate.

Photographs of the instrument are shown in Figures 1, 2, 3.

Figure 1 shows the front of the instrument with the front shutter open. Behind this shutter there is another shutter, whose time of opening can be calibrated by means of a cathode ray oscillograph and a tuning fork. Of the two cables shown one is a "release cable"; when it is pulled the shutters work in the following order:

(1) The front shutter opens and is held by a stop. When it reaches the stop, the rear calibrated shutter is released.

(2) The rear (or calibrated) shutter exposes and when the exposure is finished, the front shutter stop is released and the calibrated shutter is held by the recoil check lever. This is to prevent the shutter bouncing back and re-exposing.

(3) The front shutter closes.

Fig. 3. Crown copyright reserved. Reproduced with the permission of the Controller, H.M.S.O. Aircraft Impactor: view with cover removed to show the actuating mechanism.

When the other cable — the "rewind" or reset cable is pulled, the following operations take place:

1. The recoil check lever is disengaged.
2. The calibrated shutter is rewound.
3. The front cylindrical shutter is rewound.
4. The rewind plate returns to its normal position when the rewind cable is released.

The plate holder seen in Figure 2 consists of an aluminium sheet with pieces cut out in the vertical sides to facilitate changing plates. In the operational position this plate holder is mounted on ball-bearings (taken from a German plane shot down over Salisbury Plain) and can be turned easily when plates have to be changed.

The Sampling Plates

The surfacing of the plates used for the sampling of the drops is of the utmost importance. The plates were washed first in hot chromic-sulphuric acid solution, then rinsed in distilled water, allowed to dry in a dust-free atmosphere and finally polished

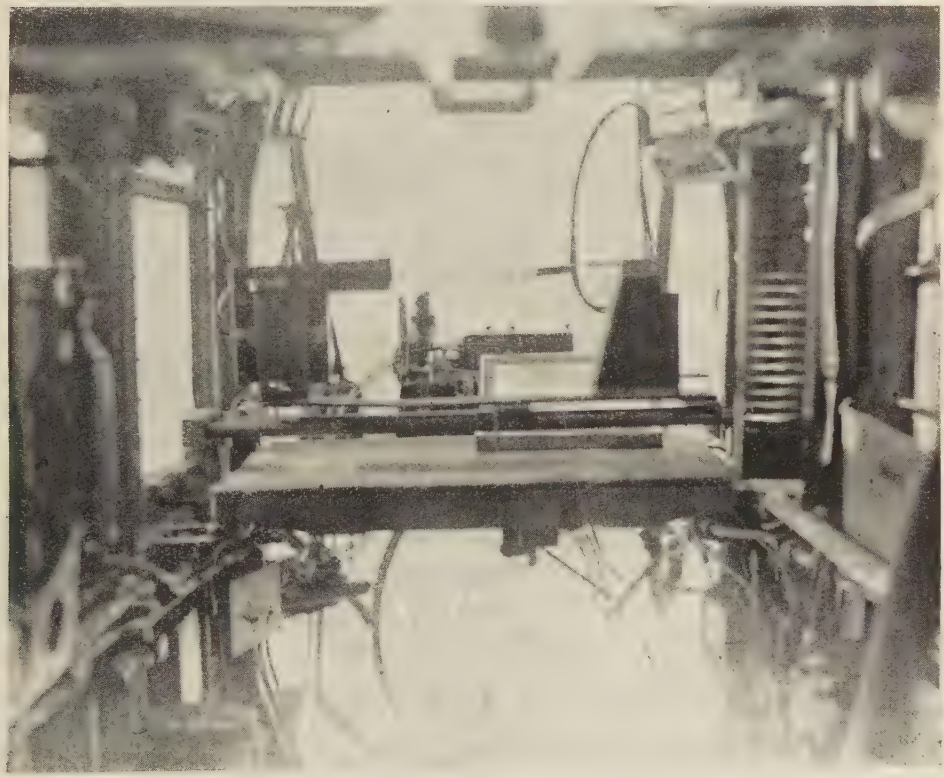

Fig. 4. Crown copyright reserved. Reproduced with the permission of the Controller, H.M.S.O. The first type of Aircraft Impactor inside aircraft. One can see the box with slides for sampling the drops.

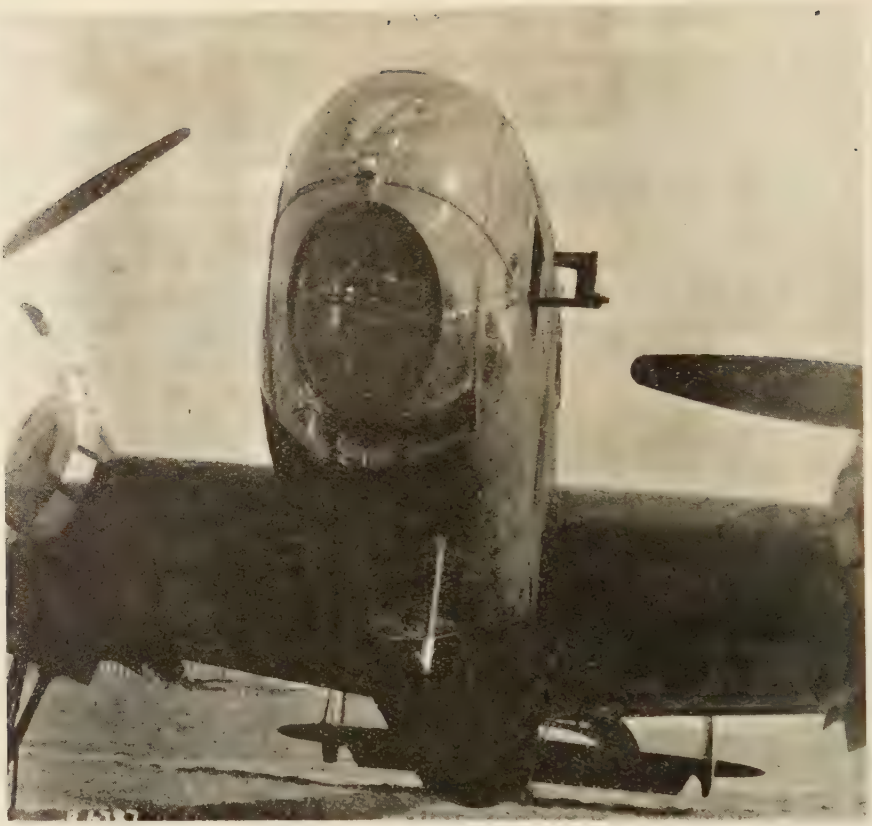

Fig. 5. Crown copyright reserved. Reproduced with the permission of the Controller, H.M.S.O. The first type of Impactor on Aircraft. The window on the right side is removed.

with untouched filter-paper. The receiving surface can then be coated with a uniform film of a substance in which the water particles can be trapped. Two methods of coating have been used: the "absolute" method and the magnesium oxide method.

I. "Absolute" method

In the first method the object is to preserve the drops in their original form by enclosing them in a surfacing substance, which must have the following properties:

1. a density not very different from that of water,
2. adequate viscosity,
3. durability and non-solubility in water,
4. colour contrast with water drops,
5. non-freezing and showing very little change of viscosity with temperature.

The matrix must be smooth and highly viscous (Benedicks and Sederholm, 1944), but of refractive index different from that of water.

The problem of proper surfacing was solved quite satisfactorily by Fuchs and Petrjanoff (1937) who found that good results can be obtained by collecting the droplets on glass slides coated with a freshly melted mixture of light mineral oil and vaseline. The proportion of the ingredients has to be varied according to air temperature and is 3:1 at 20° C. It is quite clear that the light mineral oil is the more important ingredient; its refraction is higher than that of water.

This method of coating was first used in Great Britain by the present writer during his war-time investigations on natural clouds and radiation fogs (Mazur, 1943, see also Krauss and Smith 1949, Perrie 1950, Best 1951, Brewer 1952). The light mineral oil was previously saturated with distilled water and every effort made to obtain a bubble-free film mixture.

The method adopted for the collecting of drops in natural clouds and radiation fogs (Mazur, 1944) was to place immediately after taking a sample a warmed cover-glass on the underside of which was a large drop of the same substance on the layer over the sample; the layer melted and caused the now enveloped drops to be drawn up as spheres. The cover-glasses have been warmed before use in flight by putting them on the flat surface of a lagged vessel filled with hot water at about 45—50° C. When the matrix cools and sets, the droplets can be preserved for 30 hours or more without showing any perceptible diminution in original size or change of shape.

In order to avoid a danger of coalescence and a piling up of droplets into layers when being captured on the plates, the duration of sampling has to be very short. Small distance pieces were sometimes used between slide and cover-slip to avoid squashing the larger droplets.

Some authors have obtained satisfactory results, using other mixtures: (i) Häuser and Strobl (1924) used neat's-foot oil and glycerine; (ii) Diem (1942) used two layers of different oils of different densities, collecting the drops on the interface between the layers; (iii) Bricard (1939) used mineral oil, to which organic acids had been added in order to reduce the surface tension to render easier penetration. Pure vaseline as proposed by Mason and Ludlam (1951) is definitely not suitable as a matrix for slide-surfacing for the following reasons, already stated by Houghton and Radford (1938), see also Tahakosi (1937), Mazur (1952): the surface of the vaseline layer on the glass is not smooth and when viewed under dark ground illumination it is streaky and irregular, so that some of the captured drops are always distorted and the contrast is very poor; further, the density of vaseline is 0.873 g/cc at 23° C.

The above described "absolute" method is useful as it allows the droplets to be examined microscopically and counted at leisure.

II. Magnesium Oxide method

In the second adopted method MgO is "smoked" on the glass plate by means of a gun burning magnesium ribbon, which is moved to and fro under a glass slide at such a distance that the tip of the flame just clears the glass. The uneven edges of the layer may be trimmed by scraping off with one motion of a sharp straight edge.

The white magnesium powder adhers to the glass as a smooth and soft layer with a grain size of about 0.4μ. When a drop strikes the MgO layer it penetrates the soft surface, like a round object falling into snow, and leaves a well-defined circular impression; the water, of course, evaporates. Viewed by strong transmitted light the holes are seen as bright spots on a darker background. The MgO layer should be at least as thick as the diameter of the largest droplet to be measured and preferably about twice as thick; too thick a layer is very fragile and flakes off the glass easily, May 1950.

Laboratory experiments with droplets of substance such as dibutyl phthalate, which can be sized accurately by other methods, enable drop size calibration; the ratio of diameters of drops obtained by "absolute" and magnesium oxide methods is about 0.85; the results are independent of drop size.

The MgO method has advantages over the "absolute" method in that:

(i) it is much simpler as nothing has to be done to the plate after the sample is obtained,

(ii) the craters remain without change for a long period of time (2—3 days). Disadvantages:

(i) the layer is very soft and fragile and can be damaged by high velocity air jets during exposure to the droplets; the writer found that the oxide layer is blown off the plate at a speed of about 220 m.p.h.

(ii) the method is of no value for droplets smaller than 6—8μ; the "absolute" method can show drops below 2μ diameter;

(iii) the drop of liquids other than water sometimes bounces out of the layer. To compare the results by the two methods the glass plates were coated half with MgO and half with the oil-vaseline mixture.

The magnesium oxide method is only a modification of method developed by Strazhevsky (1937), who used a uniform layer of soot smoked on to a slide during his investigations on the atomization of liquid fuel.

It is worth to mention the oldest "stain" or "absorbent paper" method, recently modified by Pauthenier and Brun (1940).

Drop Counting Technique

The droplets were counted against a Patterson-Cawood (1936) globe and circle comparator graticule, traverses being taken across a mechanical stage. For a good count about 300 drops should be taken. The number percentage in the ranges between the mean diameters corresponding to adjacent pairs of circles are then worked out and a rough curve of per cent by number up to given diameter is plotted against the diameter on a logarithmic probability paper. From a smooth curve through the plotted points a new number distribution is taken and converted into a table of total number N in the size range tabulated against size range. The mean diameter D of each size range is cubed and then multiplied by the number of drops in the rangeto give a table of ND^3 which, when reduced to a percentage gives a mass or a volume distribution. The

total mass in one hundred drops is equal to

$$M = \frac{\pi \varrho \Sigma N D^3}{6}$$

where ϱ is the density in g/cc, and $\Sigma N = 100$

The concentration in g/m^3 can be calculated and the mean volume diameter can also be derived from

$$D_v = \sqrt[3]{\frac{ND^3}{100}}$$

The sampling errors at the very small end of the spectrum of the drop size render impossible to take the total number of drops present in a cloud; however the amount of water contained in very tiny droplets is insignificant.

In his excellent theoretical paper Best (1951) showed that the size distributions of raindrops, and drop size distribution in clouds and fogs as well, may be described by the formula

$$1 - F = \exp\left[-\left(\frac{X}{a}\right)^n\right]$$

where F = the function of liquid water in the air comprised by drops with diameter less than X, and a and n are constants. Best used experimental data of the present writer and other workers (Diem 1942, 1948; Frith 1951, Hageman 1936).

The Airspeed through the Aircraft Impactor

In order to obtain trustworthy readings of airspeed in the aircraft impactor special two sets of experiments were made in the wind tunnel. For the first an old pitot static-tube, external diameter just under $\frac{1}{4}$ inch, and spacing between static and pitot holes 0.65 inches, was used. Inside a slot which measures 0.6 × 1.4 inches this distance between pitot and static holes is obviously a serious disadvantage (Peters, 1931). For the second set of experiments a specially fine pitot tube was constructed, using two stainless steel tubes each of 0.9 mm. diameter and 35 cm. length, soldered together. One advantage of the second type is that it does not disturb the flow of the air.

Measurements with both types of pitot were made at speeds of about 70 m.p.h. and 50 m.p.h. The results of the calibration are shown in Figures 6 and 7 respectively. From the latter, in which the fine pitot tube was used, it is seen that the velocity of the air sample in the slot is approximately equal to the velocity of the apparatus through the ambient air. Many experiments carried out in wind tunnel with both types of impactor have shown that there is insignificant turbulence in the channel of the apparatus and the air velocity in the channel is very little different from the velocity in the undisturbed air stream.

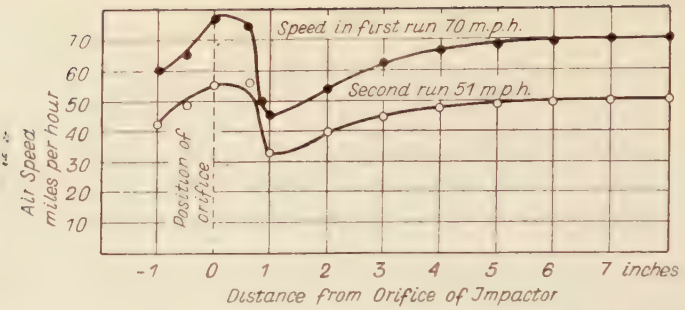

Fig. 6. Crown copyright reserved. Reproduced with the permission of the Controller, H.M.S.O. Calibration of speeds in Aircraft Impactor.

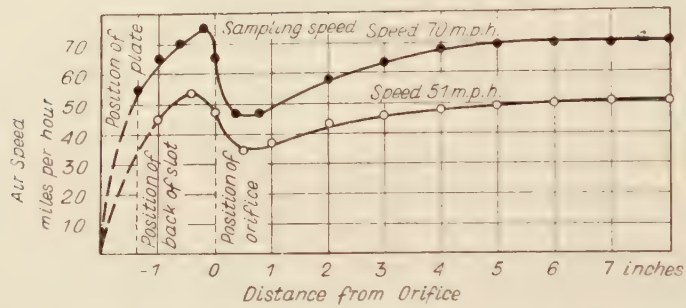

Fig. 7. Crown copyright reserved. Reproduced with the permission of the Controller, H.M.S.O. Air speeds along central axis of Aircraft Impactor (by means of a specially constructed Pitot-tube).

Results of the observations made in Natural Clouds

During the period January 1943 to May 1944 observations in natural clouds have been made over Salisbury Plain, using a Hampden bomber from Boscombe Down aerodrome, Royal Air Force Station.

Consecutive samples in the cloud formations at different points both in horizontal and vertical positions were taken during every flight.

The accuracy with which the drop diameter can be measured is limited by the resolving power of the microscope and the grain of the films. The grain size of the KODAK plates used is so small that it does not interfere with the definition of particles at least down to 1μ. It was possible during these experiments to see drops of about 1μ in diameter. No flattening effect of the drops was seen.

The curves which represent the drop size distribution or the size frequency for a cloud are very similar to a Gaussian or normal distribution curve (Maxwell curve).

The most obvious and characteristic feature common to nearly all of the curves is that there is a single and very strongly marked maximum.

In none of the samples so far examined was there more than one peak in the size distribution curve.

The distribution curves evidently become asymptotic to the axis for larger particle sizes and a definite and very sharp lower limit of drop size exists.

The clouds are not homogeneous with regard to droplet size; the diameter of drops vary from one part of a cloud to another.

The locations of the maxima of the distribution curves vary not only for different clouds but also within the same cloud.

In the interior of clouds there are larger drop sizes than in the boundary layers where the droplets must be in equilibrium with saturated ambient air.

The ranges of size are as follows: the diameter of the smallest drops was less than 1μ, and that of the largest above 100μ. The water contents in clouds varies from 0.12 to 0.41 g/m^3.

In well-established clouds the drops are larger and more uniform than in the beginning of the formation or dissipation.

The radii of drops were found to vary in the ratio about 1:100.

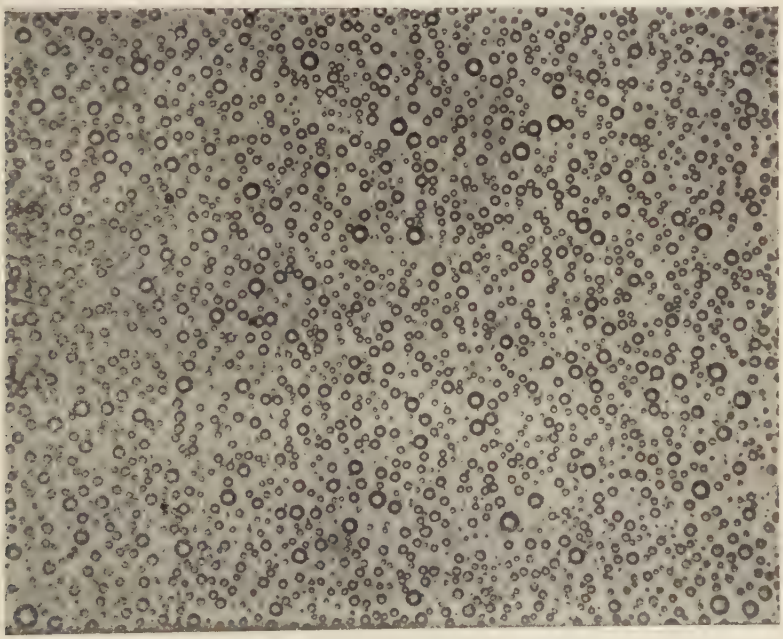

Fig. 8. Crown copyright reserved. Reproduced with the permission of the Controller, H.M.S.O.
A micrograph of cloud drops (oil — vaseline mixture)

Two micrographs of cloud drops embedded both in the grease film and in a magnesium oxide layer are shown in Figures 8 and 9 (cumulus cloud samples).
The frequency diagram for one flight, given in Figure 10, shows a typical size distribution curve for a cloud.
(Stratocumulus, flight on 27. 1. 1943, 2.000—3.000 feet).

The numerical data of this flight are given below.

First sample		*Second sample*		*Third sample*	
Diameter in microns	*Number of drops*	*Diameter in microns*	*Number of drops*	*Diameter in microns*	*Number of drops*
2	72	3	100	2	36
3	256	7	188	5	120
5	384	9	208	9	148
7	300	12	176	11	140
9	184	17	116	17	88
25	16	24	56	26	28
29	8	37	12	32	8
	1220		856		568

The numerical result of the first series of flight are tabulated below.

Number of Flight	*Genus*	*Diameter of the drops in microns*			*Concentration*
		Min.	*Mean.*	*Max.*	
1	Stratocumulus	2	24.2	100	0.16 g/m^3
2	Stratocumulus	2	14.4	37	0.12 g/m^3
3	Cumulus	9	14.7	50	0.13 g/m^3
4	Stratocumulus	3	13.1	37.5	0.12 g/m^3
5	Stratocumulus	1.5	13.3	37.5	0.15 g/m^3
6	Altostratus	1	10.6	60	0.13 g/m^3
7	Cumulus	1.4	8.8	21	0.12 g/m^3
8	Cumulus	3	10.2	18	0.41 g/m^3
9	Stratocumulus	4	9.0	16	0.38 g/m^3
10	Cumulus	6	12.6	18	0.20 g/m^3

The investigation was carried out at the Physics Department, Chemical Defence Experimental Establishment, Porton Down and all flights were made from Boscombe Down aerodrome.

From the historical point of view it is worth to mention that during the second world war investigations performed with the aid of aircraft heve been carried out by Professor Diem in Germany (for the Luftwaffe), by the present writer in England (for the Royal Air Force) and subsequently by the National Advisory Committee for Aeronautics and the Mount Observatory, Washington in the United States.

(Best 1951; Diem, 1952; 1948; Krauss und Smith, 1949; Perric, 1950).

Some experiments concerning the behaviour of the drops, especially the problem of coalescence, were carried out at the Physics Department, Imperial College of Science and Technology, London (Swinbank and Mazur, 1943).

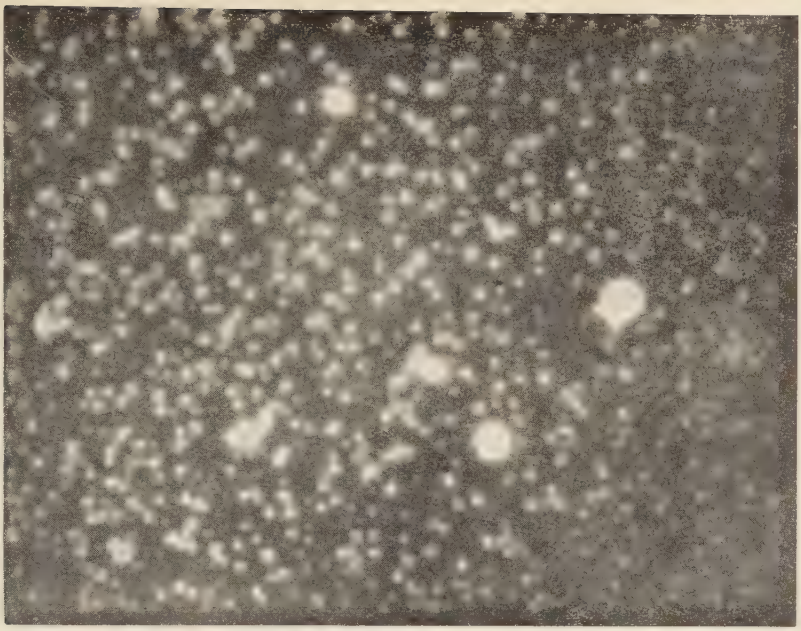

Fig. 9. Crown copyright reserved. Reproduced with the permission of the Controller, H.M.S.O.
A micrograph of cloud drops (MgO).

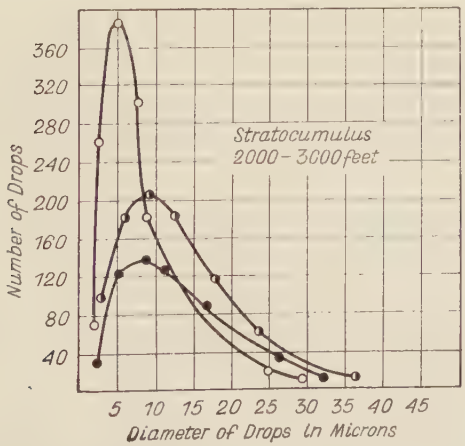

Fig. 10. Crown copyright reserved. Reproduced with the permission of the Controller, H.M.S.O.

Investigations of Fogs

As well as these investigations on clouds the present writer has carried out during the war measurements of the number, size distribution of the droplets in different types of fogs by using a Cascade Impactor (British Patent No 580717) and total water content by using an apparatus, designed by the writer and National Physical Laboratory.

The need for this information has arisen in connection with the trials which have been carried out in the dispersing radiation fog (Fog Investigation and Dispersal Operation better known as FIDO).

The investigations have been carried out during the war in the inland stations: Porton near Salisbury (Battery Hill, Beacon Hill, Tower Hill) — low stratus; river Bourne Valley, Wilts and Staines — radiation fog; coastal Royal Air Force Station St. Eval (Cornwall) — radiation fog, sea fog, low cloud, sea-spray.

The results of all investigations on fogs which have been duly submitted to the Meteorological Research Committee, Air Ministry, London, will be published in due course.

Acknowledgement

It is a pleasure to express my indebtness to Dipl. Ing. E. Szklarzyk for his helpful advice in designing the actuating mechanism of the cloud Impactor and to Dr Ing. L. Klimek for his help in preparation of this paper.

I wish also to acknowledge the assistance given in different ways by Dr H. L. Green, Head of the Physics Department, Porton Down and his staff. and the personnel from R.A.F. Station Boscombe Down, as well.

Thanks are due to the Ministry of Supply for a permission to publish this paper.

APPENDIX

Official opinion of the Air Ministry, London, concerning this work:

"The results of the investigations on clouds and fogs contributed greatly to facilitate take-offs and landings in bad weather", Destiny Can Wait, The History of the Polish Air Force in the Second World War, Foreword by Marshal of the Royal Air Force, Viscount Portal of Hungerford, London, 1949.

"Fog Investigation and Dispersal Operation, better known as FIDO, was prepared with the far-reaching collaboration of one of the Polish scientist". Destiny Can Wait, p. 341, 1949.

REFERENCES

Benedicks, C., and Sederholm, P., *Ark. Mat. Astr. Fys.* **30**A, No. 6 and **30**B, No. 5 (1944); *Nature*, **153**, 80 (1944).

Best, A. C., *Quart. J. Roy. Meteorol. Soc.*, **77**, 418 (1951).

Brewer, A. W., *Quart. J. Roy. Meteorol. Soc.*, **79**, 171 (1953).

Bricard, J., *La Metéorologie*, **15**, 83 (1939); *C. R. Acad. Sci.* (Paris), **240**, 148 (1940).

Davies, C. N., *Report on the Impactor*, P. S. Porton, 518 (1942).

Diem, M., *Ann. Hydrog.* (Berlin), **70**, 142 (1942); *Met. Rundschau*, **1**, 261 (1948).

Frith, R., *Quart. J. Roy. Meteorol. Soc.*, **77**, 10 (1951).

Fuchs, N. and Petrjanoff, J., *Nature*, **139**, 111 (1937).

Hageman, V., *Ger. Bestr. Geophys.*, **46**, 261 (1936).

Häuser, F. and Strobl, G. M., *Z. Techn. Phys.*, **5**, 154 (1924).

Houghton, H. G. and Radford, W. M., *Pap. Phys. Oceanogr. Met.*, **6**, 4 (1938).

Kraus, E. B. and Smith, B., *Austr. J. Sci. Res.*, **2**, 376 (1949).

Mason, B. J. and Ludlam, F. H., *Rep. Progr. Phys.*, **14**, 159 (1951).

May, K. R., *J. sci. Instrum.*, **27**, 128 (1950).

Mazur, J., *Report on physical properties of liquid drops*, Air Ministry, Met. Office (1941).

Report on Icing problems, Air Ministry, Met. Office (1942).

An Investigation on the Number, Size, Distribution of Water Particles and Concentration in Natural Clouds, Air Min. Met. Res. Ctee, M.R.P. 109 (1943).

An Investigation on the Number, Size, Distribution of Water Particles and Concentration in the different Types of Fogs, Air Ministry Met. Res. Ctee, M.R.P. 183 (1944).

On the Sampling of Water Droplets in Natural Clouds and in Radiation Fogs, Proc. Phys. Soc. B. LXV, 457 (1952).

Patterson, H. S. and Cawood, W., *Trans Faraday Soc.*, **32**, 1084. (1936).

Pauthenier, M., and Brun, E., *C. R. Acad. Sci.* (Paris), **211**. 295, (1940); *Ibid.* **212**, 1081 (1940).

Peters, H., *Hydro-und Aerodynamik*, *Hdb. d. Exp. Phys.*, Leipzig, Bd. 4., Teil 1. (1940).

Perrie, D. W., *Cloud Physics*, Toronto Univ. Press, 16 (1950).

Riedel, W., *Kolloid Zs.*, **1**, 31 (1938).

Strazhevsky, L., *Zh. tekh. Fiz.* (U.S.S.R.), **4**, 978 (1937).

Swinbank, W. and Mazur, J., *Some notes on physical properties of liquid drops obtained by spraying*, Air Ministry, Met. Res. Ctee, M.R.P. 98 (1943).

Tahakasi, Y., *Journ. Met. Soc. of Japan*, **15**, 3 (1937).

Wigand, A., *Met. Zs.*, XLVI (1931); *Ann. d. Hydr. und Mar.* Met. X/XI, Berlin (1931).

Wigand, A. and Schmaus, A., *Die Atmosphäre als Kolloid*, Braunschweig (1929).

ANGULAR CORRELATION THEORY WITH JACOB-WICK METHOD

By M. Micu

Institute for Atomic Physics, Bucharest

(Received August 5, 1960)

The angular correlation formula for decays of the type $A \to B + d_1$, $B \to C + d_2$ is deduced by using the development of the plane wave indicated by Jacob and Wick. The lack of Racah coefficients and of summations over the orbital angular momentum quantum numbers makes the given expression for the angular correlation simpler than the well-known expression (S. Devons and L. J. B. Goldforb 1957).

1. Introduction

Without any development in spherical harmonics some simplifications in the collision theory have been obtained by Jacob and Wick (1959).

In their paper two kinds of wave functions have been used to describe the relative motion of two particles: plane wave functions with given helicity of two particles $|\vec{p}\lambda_1\lambda_2\rangle$ and wave functions with given eigenvalues for $\vec{J}^2$, J_z and for the helicity of the two particles $|JM\lambda_1\lambda_2\rangle$.

If we denote by $\vec{p}$ the relative momentum and by $\lambda_1(\lambda_2)$ the helicity of the first (second) particle the matrix $\langle JM\lambda_1\lambda_2|\vec{p}\lambda_1\lambda_2\rangle$ which relates the two wave functions

$$|\vec{p}\lambda_1\lambda_2\rangle = \sum_{JM} |JM\lambda_1\lambda_2\rangle\langle JM\lambda_1\lambda_2|\vec{p}\lambda_1\lambda_2\rangle \tag{1}$$

apart from a factor is the matrix of the $2J+1$-dimensional irreducible representation of the rotation group, namely

$$\langle JM\lambda_1\lambda_2|\vec{p}\lambda_1\lambda_2\rangle = \frac{2J+1}{4\pi}\mathcal{D}^{J}_{M\lambda_1-\lambda_2}(\varphi\theta-\varphi) \tag{2}$$

In this paper some simplifications in the angular correlation theory are obtained by using the same procedure as the one used by Jacob and Wick in the collision theory.

2. *Angular correlation formula*

The state of the initial nucleus A is $|a; j_A m_A\rangle$. a denote all the quantum numbers of this nucleus except the spin and his projection on z-axis which are denoted by j_A and m_A. If S_1 (S_2) is the S matrix which makes the first (second) transition in the cascade decay

$$A \to B + d_1$$

$$B \to C + d_2$$

the final state ψ is

$$\psi = S_2 S_1 |a; j_A\, m_A\rangle \tag{3}$$

In the momentum-helicity representation for the relative motion we have

$$\psi = \sum_{k_1 \lambda_1 \lambda_B} S_2 |\vec{k}_1\, \lambda_1\, \lambda_B\rangle\langle \vec{k}_1\, \lambda_1\, \lambda_B |S_1|\, a; j_A\, m_A\rangle \tag{4}$$

Since the S matrix is a Lorentz invariant the final state becomes

$$\psi = \sum_{\substack{\vec{k}_1 \lambda_1 \lambda_B \\ \vec{k}_2 \lambda_2 \lambda_C}} (-1)^{j_B - \lambda_B} |\vec{k}_2\, \lambda_2\, \lambda_C;\, \vec{k}_1\, \lambda_1\rangle\langle \vec{k}_2\, \lambda_2\, \lambda_C |S_2|\, b;\, j_B - \lambda_B\rangle\langle \vec{k}_1\, \lambda_1\, \lambda_B\, |S_1|\, a; j_A\, m_A\rangle \tag{5}$$

The ket vector $|\vec{k}_2\, \lambda_2\, \lambda_C;\, \vec{k}_1\, \lambda_1\rangle$ describes the following state

— the free particle d_1 with a momentum $\vec{k}_1$ and helicity λ_1

— the free particle d_2 with a momentum $\vec{k}_2$ and helicity λ_2

— the nucleus C with a momentum $-\vec{k}_2$ and helicity λ_c.

The first momentum is referred to a frame in which the nucleus A is at rest while both the second and the third momenta are referred to a frame in which the nucleus B is at rest.

The probability to find this state in the final state is

$$W = |\sum_{\lambda_B} \langle \vec{k}_2\, \lambda_2\, \lambda_C |S_2|\, b;\, j_B - \lambda_B\rangle\langle \vec{k}_1\, \lambda_1\, \lambda_B\, |S_1|\, a; j_A\, m_A\rangle|^2 \tag{6}$$

By using eq. (1) we obtain

$$\langle \vec{k}_1\, \lambda_1\, \lambda_B\, |S_1|\, a; j_A\, m_A\rangle = \langle \vec{k}_1\, \lambda_1\, \lambda_B\, |\, j_A\, m_A\, \lambda_1\, \lambda_B\rangle\langle \lambda_1\, \lambda_B\, |\, S_1^{j_A}\, |\, a\rangle \tag{7}$$

$S_1^{j_A}$ represents, of course, the submatrix of S_1 belonging to a given angular momentum j_A.

If the parity is conserved in the decay $A \to B + d_1$ we find

$$\langle \lambda_1\, \lambda_B |S_1^{j_A}|\, a\rangle = \frac{\eta_1\, \eta_B}{\eta_A} \langle -\lambda_1 - \lambda_B |\, S_1^{j_A} |\, a\rangle \tag{8}$$

η_A, η_B and η_1 being respectively the parity factors (See M. Jacob and G. C. Wick, 1959) for the nuclei A, B and for the particle d_1. The spin of the particle d_1 is denoted by s_1.

If the initial nucleus is unpolarized and if we do not make any observation concerning the polarization of the nucleus C we have

$$W = \sum_{\lambda_B \lambda_C} |\mathcal{D}^{j_B}_{\lambda_B \lambda_C - \lambda_2}(\varphi\, \theta - \varphi)|^2 \, |\langle \lambda_2 \lambda_C | \, S_2^{j_B} \, | \, b \, \rangle \langle \lambda_1 \lambda_B \, | S_1^{j_A} | \, a \, \rangle|^2 \tag{9}$$

For polarization insensitive detectors the eq. (9) becomes

$$W = \sum_{\substack{\lambda_1 \lambda_2 \lambda_B \\ \lambda_C k}} (-1)^{\lambda_B + \lambda_C + \lambda_2} |\langle \lambda_2 \lambda_C | \, S_2^{j_B} \, | b \rangle \langle \lambda_1 \lambda_B | \, S_1^{j_A} | \, a \rangle|^2 \, C^{j_B \; j_B \; k}_{\lambda_B - \lambda_B 0} \, C^{j_B \quad j_B \; k}_{\lambda_2 - \lambda_C \lambda_C - \lambda_2 0} \, P_k(\cos\theta) \tag{10}$$

For arbitrary polarization detection we introduce the efficiency matrix ε and the density matrix ϱ of the final state (5) and from the formula $W = Spur\,(\varrho\varepsilon)$ we obtain

$$W = \sum_{k x_1 x_2} B^k_{x_1}(1)\, B^k_{x_2}(2)\, \mathcal{D}^k_{x_2 x_1}(\varphi\, \theta - \varphi) \tag{11}$$

in which ε_1 (ε_2) refers to the polarization detection of the first (second) radiation and

$$B^k_{x_1}(1) = \sum_{\lambda_1 \lambda_1' \lambda_B \lambda_B'} (-1)^{j_B - \lambda_B} \langle \lambda_1 \lambda_B | S_1^{j_A} | \, a \rangle \langle \lambda_1' \lambda_B' | S_1^{j_A} | \, a \rangle^* \, C^{j_B \; j_B \; k}_{\lambda_B - \lambda_B' x_1} \langle \lambda_1' | \varepsilon_1 | \lambda_1 \rangle \, \delta_{\lambda_1 - \lambda_B \lambda_1' - \lambda_B'} \tag{12}$$

$$B^k_{x_2}(2) = \sum_{\lambda_2 \lambda_2' \lambda_C} (-1)^{\lambda_C - \lambda_2 - j_B} \langle \lambda_2 \lambda_C | S_2^{j_B} | \, b \rangle \langle \lambda_2' \lambda_C | \, S_2^{j_B} | \, b \rangle^* C^{j_B \quad j_B \; k}_{\lambda_C - \lambda_2 \lambda_2' - \lambda_C x_2} \langle \lambda_2' | \varepsilon_2 | \lambda_2 \rangle \tag{13}$$

The meaning of the angles θ, φ used in the angular correlation formula is the following: if θ_1, φ_1 define the direction of the momentum $\vec{k}_1$ in the initial (centre of mass) frame the angles θ, φ define the direction of the momentum $\vec{k}_2$ in the frame obtained from the initial frame through a rotation of Euler angles φ_1, θ_1, $-\varphi_1$ followed by a Lorentz transformation in the new z-axis direction. The Lorentz transformation is chosen in such a way that in the final frame the nucleus B is at rest.

If the masses of the nuclei A, B and C are greater than the masses of the particles d_1 and d_2 the Lorentz transformation is not necessary and θ represents the angle between the momenta of the emitted particles d_1 and d_2.

REFERENCES

Devons, S. and Goldfarb, L. J. B., *Handbuch der Physik* vol. XLII (1957).
Jacob, M. and Wick, G. C., *Ann. Phys.*, **7**, 404 (1959).

PHOTO-STIMULATED EMISSION OF EXO-ELECTRONS FROM ANODE-OXIDIZED LAYERS OF ALUMINIUM

By Tadeusz Lewowski

Chair of Experimental Physics, Wrocław University

(Received August 11, 1960; translated paper received September 25, 1960)

It is found that photostimulated emission of exo-electrons can be obtained from Al_2O_3 layers by anode-oxidation of aluminium with AC current or by appropriate thermal processing.

The long-wave limit of the photoemission observed lies within the visible spectral region. The method utilized in oxidating the Al surface was found to affect the intensity of electron emission. The emission is considered to be due to centres resembling the F centres in alkali halides.

1. Introduction

Kramer (1955) was the first to investigate the properties of anode-oxidized aluminium layers (known as eloxal layers) by methods of exo-electron emission. He irradiated the Al_2O_3 layers formed on the surface of aluminium with ultraviolet light and investigated the temperature dependence of the emission thus excited (finding no such dependence).

In an earlier note (Lewowski 1960), the present author drew attention to the fact that photo-stimulated exo-electron emission can be excited by processing, provided AC current is used in the process of forming the Al_2O_3 layers. The subsequent sections bring further results on exo-electron emission from eloxal layers.

2. Method of measurement

Samples made of technical aluminium were degreased in a dilute aqueous KOH solution and then properly rinsed with water. Electrolytic oxidation was carried out in an aqueous solution of oxalic or citric acid (of about 1% concentration), utilizing DC or AC current. Electrolysis proceeded rapidly (in several minutes) at rather high current densities (of the order of 10^{-2} A/cm^2), and was accompanied by electroluminescent light emission. Following oxidation, in order to remove the water, the samples were rinsed in acetone and dried in a current of air at room temperature (Lewowski and Sujak 1961); subsequently, they were placed under a point Geiger counter on a movable support (Fig. 1). The counter, which operated in the atmospheric air, was bounded from below with a metal grid (100 meshes per cm^2) and was provided

with a water jacket circulating water from a Höppler ultrathermostat with the aim of keeping the counter at a constant operating temperature of 40°C (Sujak 1958). An accelerating voltage of 70V was applied between the sample and the grid of the counter.

The method was designed so as to provide for the possibility of irradiating the sample with light from a tungsten bulb or a quartz mercury lamp, and of heating

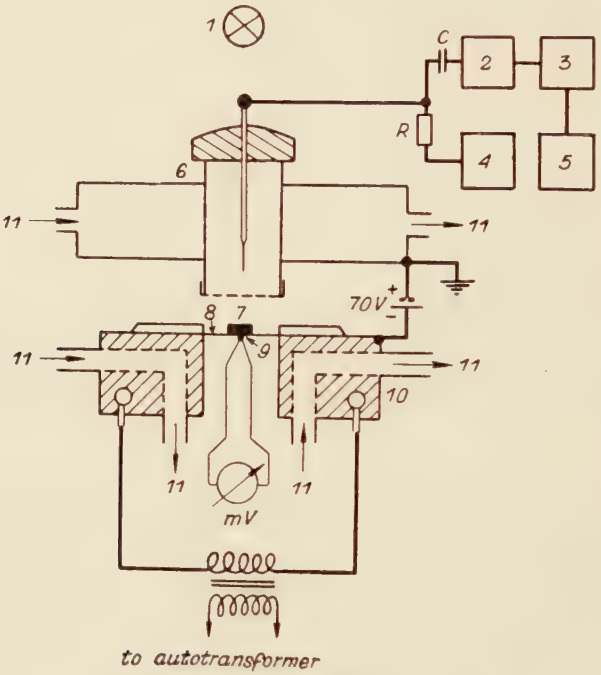

Fig. 1. Diagram of measuring circuit.

1 — 6 V/20 W bulb; 2 — amplifier; 3 — counting rate-meter; 4 — high voltage source; 5 — automatic recorder; 6 — Geiger counter with water jacket; 7 — sample; 8 — heater (kanthal sheet); 9 — thermocouple; 10 — copper cubes with current leads to heater and with water circulation; 11 — water circulation from ultrathermostat (40°C); 12 — millivoltmeter; 13 — 6 V/50 A transformer.

the sample from 40°C to about 600°C at the approximately constant rate of about 150°C per minute. For this latter aim, an electric heater of very small thermal inertia was utilized.

The electronic apparatus consisted of high voltage source, proportional amplifier, and counting rate-meter with output-connected automatic recorder (Sujak 1958).

3. *DC processing of* Al_2O_3

On oxidation of the surface of the Al samples with DC current, no exo-electron emission at room temperature was found to occur either in the dark nor in the light of a tungsten bulb. The long-wave photo-effect limit for such samples lies somewhat

above 3000 Å. If the temperature of a freshly oxidized sample, dried and placed under the Geiger counter is raised monotonously and the electron emission intensity measured simultaneously (glow-curve), the curve obtained in the dark exhibites a small maximum of the electron emission intensity at about 330°C. The emission intensity is found to increase markedly only after the temperature of 500°C has been exceeded (thermionic emission), as shown on curve 1 in Fig. 2a. If a second measurement is carried out on the same sample, the foregoing maximum tends to vanish, and electron emission is obtained only above 500°C (curve 2 in Fig. 2a).

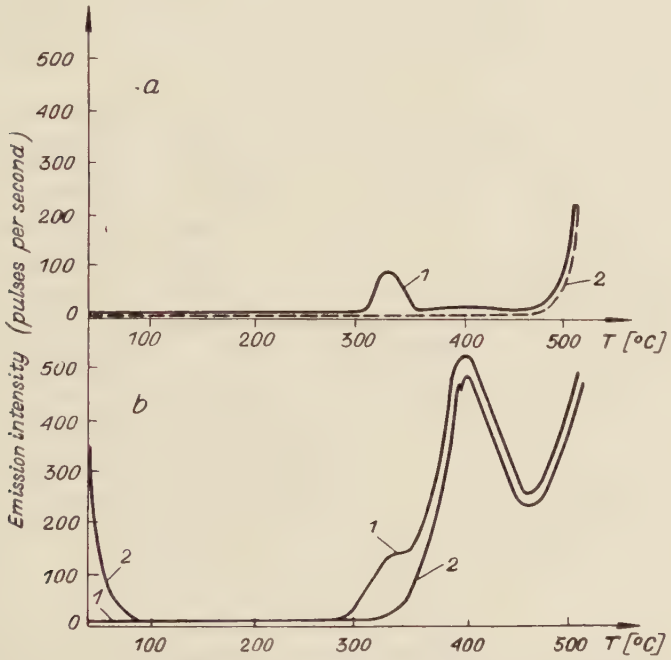

Fig. 2. Glow-curves for electrons from Al_2O_3 layers formed in the process of oxidation by DC current. a) 1 — new sample in dark; 2 — second measurement; b) 1 — new sample illuminated from bulb; 2 — second measurement.

The analogous temperature glow-curve obtained with simultaneous irradiation of the freshly-processed sample with light from the tungsten bulb exhibited two maxima that were situated near 330°C and 400°C (curve 1 in Fig. 2b). In a second measurement on the same sample, the maximum at 330°C vanishes, but the one at 400°C remains. Moreover, excitation of photostimulated exo-electron emission occurs already at room temperature (curve 2 in Fig. 2b).

This excitation is especially easily accessible to observation if, originally, heating of the sample to 400°C and cooling to 40°C have been conducted in the dark. Thermally excited photostimulated emission of exo-electrons decays very rapidly (curve 1 in Fig. 3).

The process of thermal excitation and the observation of electron photoemission can be repeated many times on one and the same sample. At a fixed temperature of about 400 °C, the intensity of photostimulated electron emission decays slowly, decreasing by some 20% during 30 minutes.

4. Al_2O_3 *formation with AC current*

As already mentioned (Lewowski 1960), on formation of Al_2O_3 layers with AC current, electron emission at incandescent bulb illumination is observed to occur at room temperature. The intensity of the emission thus excited decreases with the time as shown by curve 2 in Fig. 3. The temperature glow-curve resembles curve 2 in Fig. 2b.

5. *Effect of the degree of oxidation of the Al surface*

Experiments showed that not all electrolytes utilizable for the formation of an oxide layer yield simultaneous excitation of the sample to exo-electron emission during oxidation of Al with AC current. Electrolytes exist for which no simultaneous excitation to the emission of exo-electrons is observed notwithstanding the fact that electrolysis was accompanied by electroluminescent light emission and led to the formation of an oxide layer. The latter group of electrolytes comprises e.g. dilute aqueous solutions of $KMnO_4$, $K_2Cr_2O_7$, CrO_3, $Na_2B_4O_7$ and of other compounds rich in oxygen. Moreover, addition of a small amount of one of them to solutions of citric or oxalic acid yields samples exhibiting electron emission of an intensity many times smaller than that of samples processed in a pure solution of the respective acid.

Attempts at thermal excitation of electron emission from Al_2O_3 layers obtained in strongly oxidizing electrolytes were also unsuccessful.[1]

6. *Discussion*

The exponential decay of intensity of the photoelectron emission, and the fact that similar half-times of decay are obtained with different excitation methods, such as thermal excitation (curve 3 in Fig. 3) and oxidation with AC current (the initial part of curve 2 of Fig. 3), seem to point to the presence of similar centres of emission in either case.

The process of electrolytic oxidation of aluminium, when conducted rapidly in an acid medium at rather high current densities, provided conditions for incomplete oxidation of aluminium and hence for the arising of Schottky type defects (Grunberg and Wright 1955, and Sujak 1959). The empty oxygen lattice points can subsequently be occupied by electrons e.g. if the sample is subjected to electric discharges in a gas,

[1] The addition of even a small amount of $Na_2B_4O_7$ to the oxalic acid changes the spectral composition of the electroluminescent light, released during the formation of Al_2O_3-layer. The intensity of the yellow part decreases namely when compared with the intensity of the blue part of the light emitted. This shows that there exists a correlation between the ability of excitation of exoelectron emission and the spectral composition of electroluminescence light in the case of Al_2O_3.

or during the flow of electrolysis current in the direction of transmission (in the process of oxidation with AC current) (Lewowski 1960), or in raising the temperature of the sample. In the last case, the electrons most probably pass from the conduction band of the metal through the potential barrier at the metal-oxide contact to the trap levels of the oxide. (The conduction band of the oxide lies lower and, if there are no other full levels in the oxide, the only way of explaining the process of thermal excitation of the oxide to photo-emission within the visible range is by invoking the tunnel effect). The trap levels thus invested, whose structure resembles that of the F centres in alkali halides, can become on illumination of the sample the source of photoelectrons presenting an effective work function lesser than that for the exit of electrons from Al or from Al_2O_3 containing no such levels.

Electron emission of longer time of decay (curve 2 of Fig. 3) seems to be related to other emission centres in Al_2O_3, or to the process of etching Al (the chemical reaction, cf. Wawrzyniak and Sujak, 1960) by citric or oxalic acid. This latter hypothesis

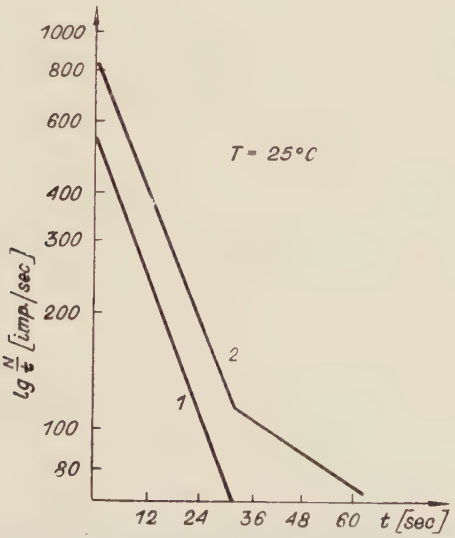

Fig. 3. Curves of decay of electron emission excited from Al_2O_3 layers. 1 — thermal excitation, 2 — excitation by formation with AC current.

seems to be the more probable one, as photo-electron emission of very great intensity and a similar time of decay was found to occur e.g. on immersing an Al sample in a dilute solution of orthophosphoric acid, H_3PO_4. On the other hand, electron emission occurring also in the dark at about 330°C in new samples is presumably related to the presence of water in the oxide lattice, notwithstanding the fact that it takes place only in the presence of an accelarating potential between the sample and the grid of the counter. Further investigation is proceeding.

The author thanks Professor B. Sujak for his discussion of the subject and for his valuable advice.

REFERENCES

Grunberg, L. and Wright, K. H. R., *Proc. Roy. Soc. A.* (London), **232**, 403 (1955).
Kramer, J., *Metalloberflaeche A*, **9**, 1 (1955); **9**, 28 (1955).
Lewowski, T., *Z. Naturforsch.*, **15a**, 90 (1960).
Lewowski, T. and Sujak, B., *Acta phys. Polon.*, **20**, 119 (1961)
Sujak, B., *Z. angew. Phys.*, **10**, 531 (1958); *Brit. J. Appl. Phys.*, **10**, 102 (1959).
Wawrzyniak, J. and Sujak, B., *Nature*, **186**, 467 (1960).

THERMAL CONDUCTIVITY CHANGES OF $ZnSO_4 \cdot 7H_2O$ BELOW 10°K

By B. Sujak*

The Clarendon Laboratory, Oxford, England

(Received Semptember 5, 1960)

Preliminary results have shown, that treatments with water and the presence of acetone vapor in the gas atmosphere in which the single crystal specimens of $ZnSO_4 \cdot 7H_2O$ were stored at room temperature, influenced their thermal conductivity measured at low temperatures below 10°K. The water increased but acetone vapor reduced the thermal conductivity below that temperature. The thermal conductivity values above 10°K always remained unafected.

Reductions of the initial thermal conductivity of about 50% due to acetone vapor could be observed at 3.5°K.

The observed phenomenon is thought to be due to changes of perfection of the specimens used, as a result of adsorption and diffusion of acetone and water molecules from and into the specimens which lead to changes in stechiometric composition of the specimens.

Introduction

Bijl (1949) found in a course of experiments on Chromium Potassium Alum $[KCr(SO_4)_2 \cdot 12H_2O]$ that the curves of the thermal resistance versus temperature resulting from different runs, but obtained with one rod did not coincide in the temperature region below 4°K. Higher values for the thermal resistance were found when the crystal was cooled down slowly. Bijl (1949) concluded that the observed phenomena were characteristic of the substance examined, rather than a consequence of the imperfect physical purity of the rods used. He further stated that it seemed to be feasible that the water molecules in the crystal lattice were responsible for this behaviour.

In this report some qualitative, preliminary results concerning similar behaviour in Zinc Sulphate Hydrate will be discussed. Because the behaviour of Zinc Sulphate Hydrate seems to be due to the changes in the physical purity of the samples used (especially the water molecule distribution), some general theoretical consideration on the thermal conductivity problem will be first outlined.

---

* On temporary leave from Zakład Niskich Temperatur Instytutu Fizyki Polskiej Akademii Nauk, Wrocław.

Theoretical considerations

In the total lattice thermal conductivity K_l the effects of transport of heat energy by waves of all different lattice frequencies are observed. To obtain a simple expression for the thermal conductivity it is necessary to average the frequency over the whole spectrum. It is convenient to introduce the kinetic formula

$$K_l = \tfrac{1}{3} c \bar{v} \Lambda \tag{1}$$

Where c is the specific heat at constant volume, $\bar{v}$ is the average phonon velocity and Λ is the phonon mean free path. By the mean free path of a phonon, we mean the distance a wave travels before its intensity is reduced to $1/e$ of its initial values (Ziman 1960).

At the lowest temperatures, below the temperature of the thermal conductivity maximum the mean free path of the phonons is mainly determined by scattering of phonons by grain boundaries and the external boundaries of the specimen and lattice defects as impurity atoms or vacancies and dislocations.

At higher temperatures the mean free path of the phonons is almost entirely determined by the phonon-phonon scattering (Peierls 1929, 1935) and the recently measured spin-phonon scattering (Rosenberg and Sujak 1960, Orbach 1960).

When the possibility of interchanges with the water of crystallization structure in a hydrate is taken into consideration it seems reasonable to assume that the changes in the specimen will take place first in its surface layer. This means that point defects (vacances or impurities) and different grain boundaries may be created in this layer. By extracting some of the water molecules from the specimen (hydrate) some vacancies will be created. By diffusion of different vapors different impurity defects will be created in the studied specimens. By these treatments the surface roughness will also be changed and this will alter the surface reflectivity.

It may be shown (Ziman 1960) that, for phonons, the surface reflectivity may influence their mean free path Λ_s as follows

$$\Lambda_s = \frac{1+p}{1-p} \Lambda_r \tag{2}$$

where p may be defined as the polish of the surface and gives a measure of the reflectivity of the surface. For a perfectly rough surface $p = 0$ and for a perfectly smooth surface $p = 1$ is put.

On the other hand if Λ_i is the mean free path associated mainly with the internal scattering by lattice imperfections, Ziman shows that in addition to boundary scattering (by assuming that the walls of the specimen are perfectly rough) the total mean free path of the phonons is given by:

$$\Lambda = \frac{3}{4\pi S_c} \iint \Lambda_i \left\{ 1 - \exp\left(- \frac{r - r_B}{\Lambda_i} \right) \right\} \cos^2 \theta \, d\theta \, dS_c \tag{3}$$

where S_c is the cross section of the specimen (rod), $d\theta$ is an element of solid angle giving the phonon path direction $(r-r_B)$ which is supposed to make an angle θ with the thermal gradient along the axis of the sample (rod).

The following formula can be also put down as a case of Matthiesen's rule:

$$\frac{1}{\Lambda} = \frac{1}{\Lambda_i} + \frac{1}{\Lambda_s} \tag{4}$$

and assuming this to be correct[1] for the first crude approach Λ will be given by

$$\Lambda = \frac{\Lambda_i \Lambda_s}{\Lambda_s + \Lambda_i} \tag{5}$$

Putting the total mean free path Λ into (1) we may write the kinetic formula for thermal conductivity as follows:

$$K_l = \frac{1}{3} c\bar{v} \frac{\Lambda_i \Lambda_s}{\Lambda_s + \Lambda_i} \tag{6}$$

Any change in the lattice perfection even if it is only in the surface layer will influence the thermal conductivity K_l because Λ_s will be affected. One has to bear in mind that the phonon reflectivity of the surface layer is not the same as the reflectivity of light at the specimen surface. Therefore adsorption, absorption and diffusion processes of various vapors on the surface and into the specimen during the time of storage at room temperature before the cooling down process starts, will influence the thermal conductivity values in the very sensitive temperature region below the lattice thermal conductivity maximum. This will occur in a way dependent on the occurrence of these processes for the given samples.

The adsorption and diffusion processes in hydrates at room temperatures occur easily. In particular the diffusion of the water molecules occurs in both directions, into or out of the specimen dependent on the atmosphere surrounding it. Therefore it seems that the hydrates are particulary sensitive specimens for this type of investigation.

Experimental

a) *The specimens*

The experiments were carried on with $ZnSO_4 \cdot 7H_2O$ single crystals with $FeSO_4 \cdot 7\,H_2O$ impurity added to the solution in which the crystals were grown. The specimen I included about 0.25% weight and specimen II about 1% weight of this impurity. The basic materials used was of the "Analar" purity grade (maximum impurity 0.006%). The specimens were cut from larger single crystals along the edges to the size of about 3 cm in lenght and 0.4 cm in square. The thermometer contacts as well

---

[1] Ziman (1960) discusses the reasons for which this formula must give spurious results by a deeper approach.

as the "cold contact" were made of copper wire and were cemented to the samples with "Araldite". On the "hot end" of the specimens a non-inductive heater coil of about 100 Ω was cemented.

b) *The method and apparatus*

The method of thermal conductivity measurement as well as the apparatus used was the very same as already described by Rosenberg (1955), they will be therefore only briefly outlined now.

Thermal conductivity measurements were taken in the temperature range between 2.5°K and 23°K using the stationary method. One end of the specimen was attached to the high pressure chamber of a Simon expansion helium liquefier with the aid of a copper wire connection. This provided the "cold contact". The other end of the specimen was heated electrically. The temperature gradient along the specimen was measured by two helium gas thermometers using a differential manometer. The two helium gas thermometers were attached to the copper contacts on the specimen. In view of the relativly high thermal conductivity of the specimens the power input to the heater was of the order of 10 to 20 milliwatts, which gave a temperature difference which in the most cases was below 0.1° K. In a few case it was as high as 0.4° K.

The measurements were carried out on two specimens. The cooling down process from room temperature proceeded in the following way. The atmospheric air surrounding the specimen mounted in the apparatus at room temperature was first pumped after the apparatus (and the sample) have been cooled down to about 90° K. By this one should avoid dehydrating the specimen. The air acted also as a heat exchange medium (a very poor one) in the cooling down process to about 90° K. The time needed to reach 90° K from room temperature was about 4 hours. After that the air was evacuated and replaced with helium exchange gas at a small pressure to continue the slow cooling down process. Liquid hydrogen temperature (20° K) was reached by the high pressure chamber of the expansion liquefier in about 1 hour. At the temperature of liquid hydrogen the measurements began. They lasted always about 4 hours until the helium bath temperature of about 2° K was reached.

c) *The results*

The results obtained with the specimen I (0.25% Fe impurity) for different, subsequend runs are collected in Fig. 1.

Run I

The curve denoted by I (+) gives the thermal conductivity results for the first run

Run II

After the measurements of the first run were ended the apparatus was warmed up to about 90° K. This took about one hour. The atmospheric air was let into the specimen space to a pressure slightly below one atmosphere. Then the temperature of the apparatus was raised to room temperature and the pressure of air in the specimen chamber was continuously aqualised to atmospheric pressure. After this the apparatus was cooled down again to liquid oxygen temperature (90° K).

In about 24 hours the air was pumped from the specimen chamber and the helium exchange gas admitted. The apparatus was cooled down to liquid hydrogen temperature (in about 1 hour) and the measurements of the thermal conductivity started for the second time.

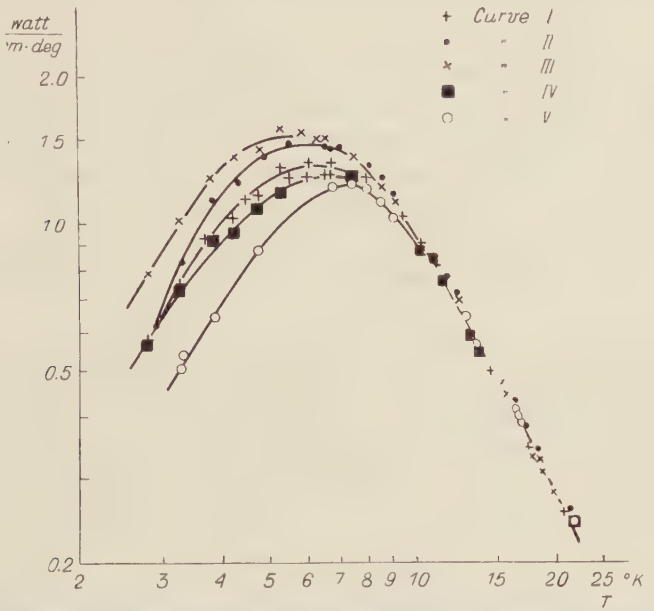

Fig. 1. Measured thermal conductivity k *versus* temperature T for sample I — $ZnSO_4.7H_2O$ (0.25% $FeSO_4$) (+) run I, (·) run II, (×) run III, (■) run IV, (o) run V (for details see text).

The results obtained are shown as curve II. It can be seen that the values of the thermal conductivity are higher in the region below about 9° K than in the case of the first run. The maximal increase of about 10% is to be seen at about 5° K.

Run III

After the measurements of the thermal conductivity values given by curve II were finished the apparatus was allowed to warm up to room temperature over-night. Then the specimen was wetted with distilled water and quickly dried with absorbent paper. After this treatment the surface of the specimen became very clear. The specimen chamber was resealed and the cooling down process started. The results obtained in this third run are given by the curve III (×).

The thermal conductivity showed a further increase especially at the lowest of measured temperatures. The increase is of about 30% at 3°K (the values given by curve II are taken as 100%).

Run IV

After the measurements of the third run were taken the apparatus was allowed to warm up again over-night to the room temperature and the specimen chamber reopened. A small amount of acetone was put in the specimen chamber (it did not touch the specimen as a liquid) and the apparatus was prepared for the next run.

After about 5 hours the cooling down process could start. The results of the following thermal conductivity measurements taken are given by curve IV (■).

A very marked decrease of the thermal conductivity below 10°K appeared with respect to the values of the curve given by run III.

Run V

The apparatus was warmed up again to about 200°K and *dry* air at atmospheric pressure was then admitted into the specimen chamber. After that, the apparatus was warmed up to room temperature and the pressure in the specimen chamber equalized to the atmospheric pressure again. Afterwards the apparatus was cooled down tp 90°K (this took about 4 hours). It was kept at 90°K for 48 hours, when the next run took place.

The results of measured thermal conductivity in that run are given by the curve V (o).

As it is to be seen a further decrease in the conductivity accured. The decrease in the conductivity was more pronounced at 3°K than at 5°K just the opposite of the case of run IV (curve IV).

It is very significant that all runs gave very coincident results from 20°K to temperatures down to about 10°K.

High vacuum conditions

To prove that in high vacuum conditions and at sufficient low temperatures (say 90°K) the specimen can be stored and the subsequent results will coincide completely the next experiment was performed and the results are given in Fig. 2.

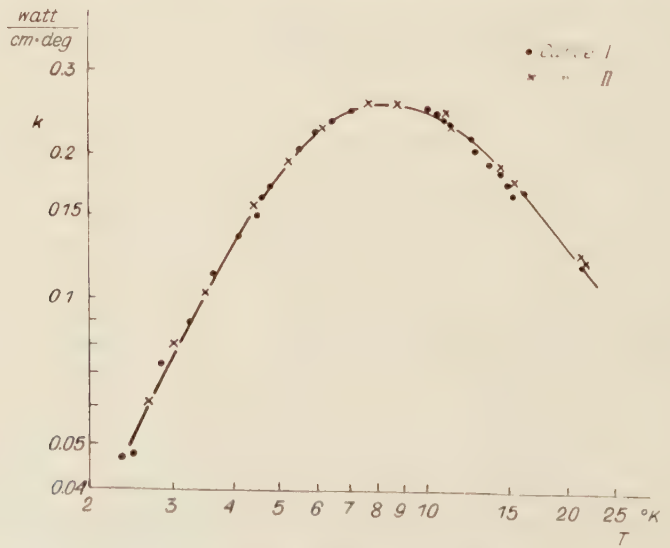

Fig. 2. Measured thermal conductivity *k versus* temperature *T* for sample II — $ZnSO_4 \cdot 7H_2O$ (1% $FeSO_4$). (·) run I, (×) run II (for details see text).

The specimen II (1% Fe impurity) was used for this purpose. The thermal conductivity was measured in the same conditions as run I in the measurements described above — curve I in Fig. 2. Afterwards the apparatus was warmed up to 90 °K and keept at that temperature for about 30 hours. During that time the high vacuum was maintained in the specimen chamber (order of 10^{-5} mm Hg).

Then the second run took place. The thermal conductivity curve obtained (curve II) coincided now with the former curve I even below 3°K.

Further runs proved also that always when the specimen lost some water of crystallization (for example after treatment with warm air) the surface became less clear and the conductivity curve was reduced on the low temperature side of the maximum.

Discussion

The qualitative results show clearly that in future studies of thermal conductivity of dielectrics (and especially hydrates) at very low temperatures below the conductivity maximum the history of the specimen before the measurements take place is essential. This concerns not only the crystallization process but even the conditions of the atmosphere at which the samples are stored.

The changes observed in the thermal conductivity values for the same sample may be ascribed to the changes in the water molecule-concentration in the samples which may lead to changes in crystalline structure or the similar behaviour, i.e. the creation of point defects by irradiation or the diffusion of alkali metals into the alkali halides — the so called *F* centers (Berman et al. 1955, 1959; Pohl 1960).

Further study is essential to find out how fast the sensitivity of the thermal conductivity measurements in the region below the maximum can be evaluated for adsorption, absorption and diffusion problems in dielectric crystals, especially hydrated crystals.

The author wish to thank very cordially Dr H.M. Rosenberg for the patient and essential guidance in introduction into the basis of the technique of thermal and electrical conductivity measurements at low temperatures and for the provision of the samples.

Opportunity is also taken to express gratitude to Professor B. Bleaney for his kind wellcome and permission to work at The Clarendon Laboratory.

The stay at The Clarendon Laboratory was financed by the Polish Academy of Sciences for which best thanks should be expressed.

REFERENCES

Berman, R., Foster, E.C. and Rosenberg, H. M., *Report on Bristol Conference on Defects in Crystalline Solids* — Physical Society, London (1955) page 321.

Berman, R., Nettley, T., Sheard, F. W., Spencer, A. N., Stevenson, R. W. H. and Ziman, J. M., *Proc. Roy. Soc.*, (London). **A253**, 403 (1959).

Bijl, D., *Physica*, **14**, 684 (1949).
Orbach, R., *Phil. Mag.*, **5**, 1303 (1960).
Peierls, R. E., *Ann. Phys.* (Leipzig), **3**, 1055 (1929), *Ann. Inst. Poincare*, **5**, 177 (1935).
Pohl, R. O., *Phys. Rev.*, **118**, 1499 (1960).
Rosenberg, H. M., *Phil. Trans.*, **A247**, 441 (1955).
Rosenberg, H. M. and Sujak, B., *Phil. Mag.*, **5**, 1299 (1960).
Ziman, J. M., *Electrons and Phonons*, The Clarendon Press, Oxford 1960.

APPROXIMATE WAVE FUNCTIONS IN THE CALCULATION OF ELECTRON EXCITATION ACCOMPANYING THE BETA-DECAY OF He^6

By Włodzimierz Kołos

Laboratory of Radiation Chemistry, Institute of Nuclear Research, Polish Academy of Sciences, Warsaw and Department of Electrochemistry, Institute of Physical Chemistry, Polish Academy of Sciences, Warsaw

(Received September 15, 1960)

The probability of non-excitation of atomic electrons in the beta-decay of He^6 has been calculated using approximate wave functions including the self-consistent field ones. The results are significantly different from those obtained with wave functions which give more accurate values of the energy.

The atomic excitation and ionization which accompany β-decay of the nucleus have been studied theoretically by many authors. However, the mean β-induced ionizations estimated theoretically do not seem to agree with the experimental values (see e.g. Schwartz 1953). In most of these calculations the atomic wave functions employed were constructed from one-electron hydrogen-like orbitals and it has been suggested that the more accurate self-consistent field (SCF) wave functions should be used to improve the theoretical results.

The purpose of the present note is to show how sensitive are the probabilities of the β-induced transitions to the form of the wave function employed in the calculation. The most convenient quantity that can be used to test various approximate wave functions is the probability of finding in the ground state the Li^+ ion resulting from the β-decay of He^6. For both systems many approximate wave functions can be found in literature.

It has been shown by Feinberg (1941) that in β-decay the main effect comes from the shaking of the atomic core due to the change of nuclear charge. Thus, in the sudden perturbation theory, the probability of finding the daughter Li^+ ion in its n-th quantum state (in the discrete or continuous spectrum) is given by

$$P_{0n} = \left| \int \varphi_0 \, \psi_n^* \, d\tau \right|^2, \tag{1}$$

where φ_0 is the ground state wave function of the helium atom, and ψ_n is the wave function for the n-th state of the Li^+ ion. P_{0n} obviously vanishes if φ_0 and ψ_n have

different symmetries. P_{00} is the probability of non-excitation, i.e. the probability of finding the Li^+ ion in its ground state. The quantities P_{0n} fulfill the following condition

$$\sum_n P_{0n} = 1, \tag{2}$$

where $\sum_n$ denotes summation over all states of the discrete spectrum and integration over continuum.

For the β-decay of He^6 the probabilities P_{0n} have been computed by Winther (1952). To calculate P_{00} he employed for He the 6 term and for Li^+ the 7 term Hylleraas' wave functions, i.e. expansions in terms of $r_1 + r_2$, $r_1 - r_2$ and $r_{12} = |\vec{r}_1 - \vec{r}_2|$. We want, however, to test simpler types of wave functions, especially those obtained by the SCF method, which are believed to be accurate and which are available or can be obtained for more complex systems. Therefore we have calculated P_{00} using for He the following wave functions

$$\varphi_{01} = N_1 e^{-\zeta(r_1+r_2)} \tag{3}$$

$$\varphi_{02} = N_2 \chi(r_1) \chi(r_2), \tag{4}$$

$$\varphi_{03} = N_3 [e^{-\zeta_1 r_1 - \zeta_2 r_2} + e^{-\zeta_1 r_1 - \zeta_1 r_2}], \tag{5}$$

$$\varphi_{04} = N_4 e^{-\zeta(r_1+r_2)} (1 + c r_{12}), \tag{6}$$

$$\varphi_{05} = N_5 e^{-\zeta(r_1+r_2)} [1 + c_1 r_{12} + c_2 (r_1 - r_2)^2], \tag{7}$$

where χ represents the SCF orbitals computed by Weiss (1958) in the form of expansions in terms of the Laguerre polynomials

$$\chi(r) = e^{-\zeta r} \sum_{m=1} a_m L^2_{m+1}(2\zeta r). \tag{8}$$

For the Li^+ ion the functions $\psi_{01}, \ldots \psi_{04}$ hawe been employed. They have the form of $\varphi_{01}, \ldots \varphi_{04}$ respectively, of course, with different parameters which in all cases have been obtained by minimizing the energy. In the SCF orbitals (8) 5 term expansions have been used; for helium also a 3 term expansion, and in this case the corresponding wave function will be denoted by φ'_{02}. The 6 and 7 term wave functions used by Winther (1952) for He and Li^+ respectively we shall denote by φ_{0w} and ψ_{0w}.

The calculation of P_{00} is straightforward and the results are presented in Table I where in the last column the value obtained by Winther (1952) is also given. In the last line we give the sums of the energies of both systems obtained with the corresponding wave functions.

Table I

Values of P_{00} calculated with various wave functions

Wave functions	φ_{01}, ψ_{01}	φ'_{02}, ψ_{02}	φ_{02}, ψ_{02}	φ_{03}, ψ_{03}	φ_{04}, ψ_{04}	φ_{05}, ψ_{04}	φ_{0w}, ψ_{0w}
P_{00}	0.7247	0.7317	0.7314	0.7110	0.7174	0.6859	0.6698
− Energy (au)	10.0700	10.0980	10.0981	10.1247	10.1516	10.1707	10.1827

The results shown in Table I are rather surprising. They suggest that the SCF wave functions give the worst values of the probability P_{00}. Even the wave functions (3), which in fact are also SCF wave functions only poor ones, give for P_{00} a value that seems to be more accurate. This is in contrast with calculations of other quantities. Thus, it is well known that the SCF wave functions yield good results when applied to calculate expectation values of the operators which depend only on the overall electron density distribution and not explicitly on r_{12}. Therefore, to test in a different way the wave functions employed in this calculation, we computed for helium the expectation values of r and r^2 using the wave functions $\varphi_{01}, \ldots \varphi_{05}$. The results are shown in Table II.

Table II

Expectation values of r and r^2 for the helium atom

Wave function	φ_{01}	φ_{02}'	φ_{02}	φ_{03}	φ_{04}	φ_{05}
r (au)	0.8889	0.9265	0.9273	0.9379	0.8970	0.9237
r/r_{ac}	0.9563	0.9968	0.9977	1.0090	0.9650	0.9937
r^2 (au)	1.0535	1.1803	1.1849	1.2473	1.0772	1.1736
r^2/r_{ac}^2	0.8827	0.9889	0.9928	1.0450	0.9025	0.9833

The ratios of the computed expectation values to the accurate ones (Kołos, Roothaan and Sack 1960) are also given. In this case the SCF wave functions yield very good results, more accurate than those obtained with other approximate wave functions which are better for calculation of the energy.

We must admit that probably the value of P_{00} obtained with the SCF wave functions is the least accurate one. However this is not certain. A wave function with most variational parameters which partly accounts for electron correlation and gives the best energy does not always describe in the best way all properties of the system. Let us consider e.g. the probability of finding both electrons of the helium atom close to the nucleus. This probability is given by $|\varphi_0(0, 0)|^2 \, d\tau$ where $\varphi_0(0, 0)$ is the number obtained from the wave function $\varphi_0(r_1, r_2)$ by putting $r_1 = r_2 = 0$. The value of the wave function for $r = 0$ plays an important role in the theory of K- or L-capture (see e.g. Odiot 1958). The values of $\varphi_{0i}(0, 0)$ and $\psi_{0i}(0, 0)$ obtained from some wave functions used in the previous calculation are given in Table III, where Ψ_{0i} denotes φ_{0i} or ψ_{0i} for He and Li^+ respectively. For helium they show the same type of regularity as the previously computed probabilities P_{00}. The results obtained with the simplest wave functions of type (3) are intermediate between the values corresponding to the SCF wave functions and those used by Winther (1952).

Table III

Values of the He and Li^+ ground state wave functions for $r_1 = r_2 = 0$

Wave function	Ψ_{01}	Ψ_{02}'	Ψ_{02}	Ψ_{03}	Ψ_{0w}
He	1.530	1.783	1.800	1.418	1.388
Li^+	6.179		6.843	5.926	6.219

Table IV

Values of the Kinoshita wave functions for $r_1 = r_2 = 0$

Number of terms	1	6	10	18	22	34	39
φ_0 (0,0)	1.530	1.388	1.371	1.923	1.9283	1.9303	1.9309

It seems natural to expect that when the electron correlation is taken into account in the wave function the probability that both electrons are simultaneously at the nucleus decreases. However, we see that this is not true for Li^+. In Table IV we give some additional values of φ_0 (0, 0) obtained from the more accurate wave functions computed by Kinoshita (1957) for the ground state of the helium atom. The 6 term wave function used by Winther also belongs to this series, as well as the simplest wave function (3), and for comparison the corresponding results are included in the Table. The results are again rather unexpected ones. We see that more than 20 terms are needed to obtain a value which is probably (but not necessarily) the most reliable, and that this value is higher than that obtained with the SCF wave functions. Thus the effect of electron correlation in the He atom on the ratio of the probabilities of K- and L-captures, found by Odiot (1958), may be reduced if more accurate wave functions are employed in the calculation. The computation of the probability P_{00} should also be carried out with much more accurate wave functions before concluding about the applicability of the SCF wave functions to this problem.

My thanks are due to Mr. A. Weiss for sending the unpublished results of his self-consistent field calculations.

REFERENCES

Feinberg, E. L., *J. Phys.*, (U.S.S.R.) **4**, 423 (1941).
Kinoshita, T., *Phys. Rev.*, **105**, 1490 (1957).
Kołos, W., Roothaan, C. C. J. and Sack, R. A., *Rev. mod. Phys.*, **32**, 178 (1960).
Odiot, J., *Théses*, Université de Paris (1958).
Schwartz, H. M., *J. chem. Phys.* **21**, 45 (1953).
Weiss, A., *Unpublished results*, The University of Chicago (1958).
Winther, A., *K. Danske Vidensk. Selsk. Mat.-fys. Medd.*, **27**, No. 2 (1952).

REVIEWS OF BOOKS

BEITRÄGE ZUR PHYSIK UND CHEMIE DES 20 JAHRHUNDERTS

LISE MEITNER, OTTO HAHN, MAX VON LAUE

zum 80 Geburtstag

Herausgegeben von O. r. Frisch. F. A. Paneth, F. Laves, P. Rosbaud. Friedrich Vieweg& Sohn, Braunschweig, 1959, 285 S.

Dieses Buch ist ein Gedenkbuch, dem 80 Gebrurtstag drei Nobelpreisträger, Lise Meitner, Otto Hahn und Max von Laue gewidmet. Es enthält drei Serien von Artikeln, deren Inhalt mit den wissenschaftlichen Forschungen der oben genannten Gelehrten eng verbunden ist.

Manche Artikel berichten über die Geschichte der Forschung der vielfältigen Gebiete, in denen die Jubilare wissenschaftlich gearbeitet haben: oft ist die Geschichte bis zu den neuesten Entdecungen geführt. Interessant sind auch die Artikel, welche die persönlichen Erinnerungen der Mitarbeiter der Jubilare beschreiben.

Der erste Teil des Buches, Lise Meitner gewidmet, enthält 7 Artikel über manche Probleme der α und β-Radioaktivität. Im ersten Artikel dieser Serie beschreibt A. Przibram seine persönliche Erinnerungen an das alte Physikalische Institut in Wien. Dann folgt ein Artikel von S. Rosenblum über die magnetischen Spektren der Teilchen. W. Heitler berichtet über die Geschichte des Durchgangs der γ-Strahlung durch die Materie vom theoretischen Standpunkte aus und endet seinen Artikel mit den Bemerkungen über nicht-lokale Theorie.

W. Gentner hat die Geschichte der frühen Forschungen über γ-Strahlung dargestellt. Dann folgt ein längerer und besonders interesantes Artikel von C. S. Wu über die Geschichte der Forschung des β-Zerfalls, der mit der Darstellung der Nichterhaltung der Parität in schwachen Wechselwirkungen endet.

H. Olsen und H. Wergeland berichten über Probleme, die mit Bremsstrahlung verbunden sind. Der erste Teil endet mit dem Artikel vom A. Flamenfeld über die Geschiche der Isomerie der Atomkerne.

Der zweite Teil des Buches besteht aus 9 Artikeln über chemische Probleme der Radioaktivität, die mit Arbeiten von Otto Hahn verbunden sind. Der erste Artikel dieser Serie enthält die Erinnerungen K. E. Zimen über Kaiser Wilhelm Institut für Chemie.

Dann folgen: ein Artikel von A. C. Pappas über radiochemische Eigenschaften der kurzlebigen Produkte der Spaltung der Atomkerne und kurze Bemerkungen von B. Karlik über Szintillationsspektrometrie.

G. T. Seaborg beschreibt die Geschichte der frühen radiochemische Forschungen von Plutonium und G. von Hevesy berichtet über die Anwendung des radioaktiven Eisens in der Biologie. Es folgen die Artikel über die Anwendung der radioaktiven Isotope bei der Forschung des Kristallwachstums (N. Riehl), in der Geochemie (H. J. Born) und Technologie der Farbstoffe (H. Baddenhausen, H. Götte und L. Wiesner).

Der dritte Teil des Buches ist Max von Laue gewidmet und enthält 10 Artikel über die Anwendung der Röntgenstrahlen in der Kristalographie und Chemie. Nach den kurzen Artikeln von P. P. Ewald und W. L. Bragg, die den historischen Charakter haben, folgt ein längerer Artikel von S. Laves über Kristallstruktur und Kristallchemie von Elementen und metallischen Verbindungen.

In zwei Artikeln besprechen A. Guinier und H. Jagodziński die Struktur der Kristalle und Mischkristalle. K. Lonsdale schreibt über die schwingenden Atome in Kristallen. Zwei Artikel von W. Hoppe und R. Hosenmann besprechen die Probleme der Forschung der Struktur von Kristalle und Molekülen mit Hilfe von Röntgenstrahlen. Diese Serie schliessen zwei Artikel von J. M. Bijvoet und G. Bormann über den Durchgang der Röntgenstrahlen.

Die Mannigfaltigkeit der Themen die in diesem Gedenkbuch dargestellt sind, ist so verschieden, dass sowohl ein Physiker, wie auch ein Chemiker und Kristalograph wird sicher einen Artikel finden, der ihn interesieren wird.

Bronisław Średniawa

LETTERS TO THE EDITOR

MODIFIED DERIVATION OF DISPERSION LAW FOR LONG SPIN WAVES IN ANTIFERROMAGNETIC REGULAR SUPERSTRUCTURES

By Henryk Cofta

Institute of Theoretical Physics, A. Mickiewicz University, Poznań

and

Ferromagnetics Laboratory, Institute of Physics, Polish Academy of Science, Poznań

(Received November 21, 1960)

In one of our previous papers (Cofta 1959) we have derived by the semiclassical method a general dispersion formula for spin waves in ferri- and antiferrimagnets, which holds for all translational (i.e. Bravais) magnetic lattices with regular[1] superstructures and which goes over into formula for antiferromagnets in the case of equal opposite spins. Its validity for arbitrary propagation vector $\boldsymbol{k}$ is rather apparent; the spin wave theory in the harmonic oscillator approximation is valid only for long spin waves for which the interactions between spin waves may be neglected. This means, that one must always confine himself to small values of k and consequently one use practically the approximate power series expansion for small k in all applications of dispersion law.

The purpose of the present paper is to show, that an direct derivation of such approximate dispersion formula is much simpler than the derivation of the apparently strict one and then its expansion. The direct way used here consists in the well known treating of atomic spins $\boldsymbol{S}_m$ as distributed in a continuous manner over the crystal[2]. Such an approach permits to express aproximately the spin $\boldsymbol{S}(\boldsymbol{m}+\boldsymbol{r})$ in the position $\boldsymbol{m}+\boldsymbol{r}$ by the first three terms of a Taylor expansion as follows

$$\boldsymbol{S}_{m+r} \approx \boldsymbol{S}_m + \left(\frac{d\boldsymbol{S}}{d\boldsymbol{m}}\right)_m \odot \boldsymbol{r} + \frac{1}{2}\left(\frac{d^2\boldsymbol{S}}{d^2\boldsymbol{m}}\right)_m \odot (\boldsymbol{r} \oplus \boldsymbol{r}) \tag{1}$$

[1] The rigorous definition of the regular superstructures may be found in the paper by Cofta (1960 b),

[2] See for example Nordheim (1934), page 857 (the case of ferromagnetic chain) or H. Kaplan (1952) (the case of ferrimagnetic spinel)

where the symbol $\oplus$ is used for dyadic multiplication of two vectors, the symbol $\odot$ however denotes a multiplication of two tensors, which contracts the product to a vector (note that $d^2\boldsymbol{S}/d\boldsymbol{m}^2$ is a tensor of the third order).

Let us denote by $\boldsymbol{A}$ and $\boldsymbol{B}$ the dimensionless vectors of atomic spin in the one and in the other sublattice respectively. The Heisenberg-Dirac exchange Hamiltonian leads to the following equations of motion (Herring, Kittel 1951) in the semiclassical approximation[3]:

$$\left.\begin{aligned}\hbar\dot{\boldsymbol{A}}_{\boldsymbol{m}} &= \boldsymbol{A}_{\boldsymbol{m}} \times \Big[\hbar\gamma\boldsymbol{H}_A + 2\sum_{\boldsymbol{r}}^{+} J_{\boldsymbol{r}}\boldsymbol{A}_{\boldsymbol{m}+\boldsymbol{r}} + 2\sum_{\boldsymbol{r}}^{-} J_{\boldsymbol{r}}\boldsymbol{B}_{\boldsymbol{m}+\boldsymbol{r}}\Big] \\ \hbar\dot{\boldsymbol{B}}_{\boldsymbol{m}} &= \boldsymbol{B}_{\boldsymbol{m}} \times \Big[-\hbar\gamma\boldsymbol{H}_A + 2\sum_{\boldsymbol{r}}^{+} J_{\boldsymbol{r}}\boldsymbol{B}_{\boldsymbol{m}+\boldsymbol{r}} + 2\sum_{\boldsymbol{r}}^{-} J_{\boldsymbol{r}}\boldsymbol{A}_{\boldsymbol{m}+\boldsymbol{r}}\Big]\end{aligned}\right\} \tag{2}$$

Here $\boldsymbol{H}_A$ is the effective field of magnetic anisotropy, γ — the magnetomechanical ratio ($\gamma<0$), $\boldsymbol{m}$ and $\boldsymbol{r}$ — the positions of lattice points, and $J_{\boldsymbol{r}}$, the exchange (or superexchange) integral between spins localized in points $\boldsymbol{m}$ and $\boldsymbol{m}+\boldsymbol{r}$ (which does not depend upon $\boldsymbol{m}$). Hence, in the antiferromagnetic case we deal with two interpenetrating spin fields $\boldsymbol{A}(\boldsymbol{m})$ and $\boldsymbol{B}(\boldsymbol{m})$. Using the expansion (1) for both $\boldsymbol{A}_{\boldsymbol{m}+\boldsymbol{r}}$ and $\boldsymbol{B}_{\boldsymbol{m}+\boldsymbol{r}}$ we obtain for (2):

$$\left.\begin{aligned}\hbar\dot{\boldsymbol{A}} &= \boldsymbol{A} \times \left[\hbar\gamma\boldsymbol{H}_A + \frac{d^2\boldsymbol{A}}{d\boldsymbol{m}^2} \odot \sum^{+} J_{\boldsymbol{r}}(\boldsymbol{r}\oplus\boldsymbol{r}) + 2\boldsymbol{B}\sum^{-} J_{\boldsymbol{r}} + \frac{d^2\boldsymbol{B}}{d\boldsymbol{m}^2} \odot \sum^{-} J_{\boldsymbol{r}}(\boldsymbol{r}\oplus\boldsymbol{r})\right] \\ \hbar\dot{\boldsymbol{B}} &= \boldsymbol{B} \times \left[-\hbar\gamma\boldsymbol{H}_A + \frac{d^2\boldsymbol{B}}{d\boldsymbol{m}^2} \odot \sum^{+} J_{\boldsymbol{r}}(\boldsymbol{r}\oplus\boldsymbol{r}) + 2\boldsymbol{A}\sum^{-} J_{\boldsymbol{r}} + \frac{d^2\boldsymbol{A}}{d\boldsymbol{m}^2} \odot \sum^{-} J_{\boldsymbol{r}}(\boldsymbol{r}\oplus\boldsymbol{r})\right]\end{aligned}\right\} \tag{3}$$

These equations are satisfied by the wave-precessional solutions:

$$\left.\begin{aligned}\boldsymbol{A} &= R_1(\boldsymbol{j}_x - i\boldsymbol{j}_y)\exp i(\boldsymbol{k}\boldsymbol{m} + \omega t) + S\boldsymbol{j}_z \\ \boldsymbol{B} &= R_2(\boldsymbol{j}_x - i\boldsymbol{j}_y)\exp i(\boldsymbol{k}\boldsymbol{m} + \omega t) - S\boldsymbol{j}_z\end{aligned}\right\} \tag{4}$$

assuming that the field $\boldsymbol{H}_A$ has the z-direction. The substitution of (4) into (3) yields two simultaneous equations for the amplitudes R_1 and R_2:

$$\left.\begin{aligned}R_1[S(F-\varkappa) + E_A + \hbar\omega] + R_2 S(G-\varkappa) &= 0 \\ R_1 S(G-\varkappa) + R_2[S(F-\varkappa) + E_A - \hbar\omega] &= 0\end{aligned}\right\} \tag{5}$$

where following abbreviations are used:

$$\left.\begin{aligned}E_A &= \hbar\gamma H_A^z = \hbar|\gamma|\, H_A \\ F(\boldsymbol{k}) &= \boldsymbol{k}\oplus\boldsymbol{k}\cdot\sum^{+} J_{\boldsymbol{r}}(\boldsymbol{r}\oplus\boldsymbol{r}) = \sum^{+} J_{\boldsymbol{r}}(\boldsymbol{k}\boldsymbol{r})^2 \\ G(\boldsymbol{k}) &= \boldsymbol{k}\oplus\boldsymbol{k}\cdot\sum^{-} J_{\boldsymbol{r}}(\boldsymbol{r}\oplus\boldsymbol{r}) = \sum^{-} J_{\boldsymbol{r}}(\boldsymbol{k}\boldsymbol{r})^2 \\ \varkappa &= 2\sum^{-} J_{\boldsymbol{r}}\end{aligned}\right\} \tag{6}$$

[3] As to the details see the paper by Cofta 1959 and 1960 a

The secular equation of (5) leads to the dispersion relation for spin waves:

$$|\hbar\omega| = \sqrt{[E_A + S(F-\varkappa)]^2 - S^2(G-\varkappa)^2} \tag{7}$$

which holds for arbitrary regular superstructure and can be obtained also by expanding all functions $\cos(\boldsymbol{kr})$ in the Ziman's (1952) dispersion law (derived using the Holstein-Primakoff formalism) or in that by Cofta (1959) (derived using the semiclassical formalism).

We may bring the derived formula into a more convenient form taking into account that for small k

$$F \sim G \ll \varkappa \tag{8}$$

Then, we may neglect the k^4 terms obtaining finally

$$|\hbar\omega| = [aF(\boldsymbol{k}) + bG(\boldsymbol{k}) + c]^{1/2} \tag{9}$$

where

$$\left.\begin{aligned} a &= 2S(E_A - S\varkappa) \\ b &= 2S^2\varkappa \\ c &= E_A(E_A - 2S\varkappa) \end{aligned}\right\} \tag{10}$$

This form is appropriate among other things for studying kinematical properties of spin waves in regular antiferromagnetics superstructures (see e.g. Cofta 1960a).

REFERENCES

Cofta, H., *Acta phys. Polon.*, **18**, 215 (1959).

Cofta, H., *Thesis* A. Mickiewicz University 1960 a.

Cofta, H., *Acta phys. Polon.*, **19**, 759 (1960 b).

Kaplan, H., *Phys. Rev.*, **86**, 121 (1952).

Nordheim, L., *Muller — Pouillet's Lehrbuch d. Physik*, 11-th. Ed. Vol. IV, 1, p. 857, Braunschweig 1934.

Ziman, J. M., *Proc. Phys. Soc.* (London), **65**, 540 (1952).